Manuscript prepared for Geosci. Model Dev.
Date: 6 June 2018

PCR-GLOBWB 2: a 5 arc-minute global hydrological and water resources model

Edwin H. Sutanudjaja[1], Rens van Beek[1], Niko Wanders[1], Yoshihide Wada[1,2], Joyce H.C. Bosmans[1], Niels Drost[3], Ruud J. van der Ent[1], Inge E. M. de Graaf[4], Jannis M. Hoch[1,5], Kor de Jong[1], Derek Karssenberg[1], Patricia López López[1,5], Stefanie Peßenteiner[6], Oliver Schmitz[1], Menno W. Straatsma[1], Ekkamol Vannametee[7], Dominik Wisser[8,9], and Marc F. P. Bierkens[1,10]

1 Department of Physical Geography, Faculty of Geosciences, Utrecht University, Utrecht, The Netherlands
2 International Institute for Applied Systems Analysis, Laxenburg, Austria
3 Netherlands eScience Center, Amsterdam, The Netherlands
4 Chair of Environmental Hydrological Systems, Faculty of Environment and Natural Resources, University of Freiburg, Freiburg, Germany
5 Unit Inland Water Systems, Deltares, Delft, The Netherlands
6 Department of Geography and Regional Science, University of Graz, Graz, Austria
7 Department of Geography, Chulalongkorn University, Bangkok, Thailand
8 Food and Agriculture Organization of the United Nations, Rome, Italy
9 Institute for the Study of Earth, Oceans, and Space, University of New Hampshire, New Hampshire, USA
10 Unit Soil and Groundwater Systems, Deltares, Utrecht, The Netherlands

Correspondence to: E. H. Sutanudjaja (E.H.Sutanudjaja@uu.nl)

Abstract

We present PCR-GLOBWB 2, a global hydrology and water resources model. Compared to previous versions of PCR-GLOBWB, this version fully integrates water use. Sector-specific water demand, groundwater and surface water withdrawal, water consumption and return flows are dynamically calculated at every time step and interact directly with the simulated hydrology. PCR-GLOBWB 2 has been fully rewritten in Python and PCRaster-Python and has a modular structure, allowing easier replacement, maintenance, and development of model components. PCR-GLOBWB 2 has been implemented at 5 arc-minute resolution, but a version parameterized at 30 arc-minute resolution is also available. Both versions are available as open source codes on https://github.com/UU-Hydro/PCR-GLOBWB_model. PCR-GLOBWB 2 has its own routines for groundwater dynamics and surface water routing. These relatively simple routines can alternatively be replaced by dynamically coupling PCR-GLOBWB 2 to a global two-layer groundwater model and 1D-2D-hydrodynamic models, respectively. Here, we describe the main components of the model, compare results of the 30 arc-minute and the 5 arc-minute versions and evaluate their model performance using GRDC discharge data. Results show that model performance of the 5 arc-minute version is notably better than that of the 30 arc-minute version. Furthermore, we compare simulated time series of total water storage (TWS) of the 5 arc-minute model with those observed with GRACE, showing similar negative trends in areas of prevalent groundwater depletion. Also, we find that simulated total water withdrawal, matches reasonably well with reported water withdrawal from AQUASTAT, while water withdrawal by source and sector provide mixed results.

1 Introduction

The last decades saw the development of an increasing number of global hydrological models (GHMs), e.g. VIC (Liang et al., 1994, Nijssen et al., 2001), WMB (Fekete et al., 2002), WaterGAP (Döll et al., 2003), H08 (Hanasaki et al., 2008a, Hanasaki et al., 2018), MAC-PDM (Gosling and Arnell, 2011) (see Bierkens et al., 2014, Bierkens, 2015 and Kauffeldt et al. 2016 for a more extensive list, also including land surface models). GHMs have become essential tools to quantify and understand the global terrestrial water cycle, as they simulate the distributed hydrological response to weather and climate variations at higher resolution (typically $0.5^o \times 0.5^o$) than used previously in general circulation models (GCMs), with more sophisticated runoff generation processes and river routing. As such, global hydrological models have been used for medium-range to seasonal flood forecasting (Bierkens and van Beek, 2009, Alfieri et al., 2013, Candogan Yossef et al., 2013) as well as for a myriad of water-related global change assessments. Examples are: the projection or estimation of future flood and drought events (Sperna-Weiland et al., 2012, Dankers et al., 2013, Prudhomme et al., 2013, Wanders et al. 2015, Wanders and Wada, 2016), current and future flood hazard and risk (Pappenberger et al., 2012, Hirabayashi et al., 2013, Ward et al., 2013, Winsemius et al., 2013, 2016), global groundwater depletion (Wada et al., 2010, Gleeson et al., 2012), the contribution of terrestrial water stores to global sea level change (Konikow, 2011, Wada et al., 2012, Pohkrel et al., 2013), current and future water scarcity under climate change and increasing population growth (Hanasaki et al., 2008b, Wada et al., 2011a, 2011b, Schewe et al., 2014, Haddeland et al., 2014, Wada and Bierkens, 2014), tele-connections between climate oscillations and water availability (Wanders and Wada, 2015), the impact of land use change on global water resources (Rost et al., 2008, Sterling et al., 2015, Bosmans et al., 2017) and trends in surface water temperature and cooling water potential (van Beek et al., 2012, van Vliet et al., 2012). More recently, the output from global hydrological models has been extended to study socioeconomic impacts, such as virtual water trade (Konar et al., 2013, Dalin et al., 2017) and future agricultural production (Elliott et al., 2013). These applications show that GHMs have become invaluable tools in support of global change research and environmental assessments.

PCR-GLOBWB (PCRaster GLOBal Water Balance) (van Beek and Bierkens, 2009, van Beek et al. 2011) is one of the recently developed GHMs. PCR-GLOBWB is a grid-based global hydrological model developed at the Department of Physical Geography, Faculty of Geosciences, Utrecht University, the Netherlands. The model, describing the terrestrial part of the hydrological cycle, was first introduced in a technical report by van Beek and Bierkens (2009) and then formally published in a paper of van Beek et al. (2011), focusing on global water availability issues. PCR-GLOBWB was originally developed to solve the global daily surface water balance with a spatial resolution of 30 arc-minutes (about 50 km by 50 km at the equator) and compare the resulting fresh water availability with monthly sectoral water demand in order to assess global-scale water scarcity (van Beek et al., 2011, Wada et al., 2011a,b). In this first version of PCR-GLOBWB (called PCR-GLOBWB 1 hereafter), similar to other global-scale hydrological models, water demand and water availability are treated independently, i.e. without direct feedback between human water use and other terrestrial water fluxes (e.g. Döll and Siebert, 2002, Wisser et al., 2010). Since it was first introduced, PCR-GLOBWB has been applied extensively in global water resources assessment studies. For instance, a recent search on Scopus (accessed on 13 April 2018) on the key-word "PCR-GLOBWB" yielded 113 publications with collectively over 2500 citations. Since the first version, several new

model features have been introduced such as a comprehensive water demand and irrigation module (Wada et al., 2011b, 2014), a scheme for dynamic allocation of sectoral water demand to available surface water and groundwater resources and the associated calculation of return flow (de Graaf et al., 2014). These features essentially introduced a two-way interaction between water demand, water withdrawal, water consumption and availability, particularly over irrigated areas where water demand is large and return flow is significant. Nevertheless, all of these preceding studies using PCR-GLOBWB were performed at a relatively coarse resolution of 30 arc-minutes, limiting their sub-regional or local applications. Additionally, some added functionalities, such as the possibility to couple the land surface component of PCR-GLOBWB to a global MODFLOW-based groundwater model (Sutanudjaja et al., 2011, 2014, de Graaf et al., 2015, 2017) and an extension to simulate surface water temperature (van Beek et al., 2012), were incorporated in different versions based on the original PCR-GLOWB 1, leading to divergent model code development.

The objective of this paper is to summarize and present the new version of the model, PCR-GLOBWB 2, which consolidates all components that have been developed since the original version of the model was first introduced (van Beek et al., 2011). The new version of the model, PCR-GLOBWB 2, which is able to simulate the water balance at a finer spatial resolution of 5 arc-minutes, supersedes the original PCR-GLOBWB 1, which has a resolution of 30 arc-minutes only[1]. The finer resolution of PCR-GLOBWB 2 allows a much better representation of the effects of spatial heterogeneity in topography, soils, and vegetation on terrestrial hydrological dynamics (Wood et al., 2011, Bierkens et al., 2014). Likewise, it provides a better resolution for visualization that allows stakeholders and decision makers to assess model simulation output more easily and directly for the places they are specifically interested in (Sheffield et al., 2010, Beven and Cloke, 2012). To assess the possible improvements, this paper also presents the first evaluation results from the simulation of PCR-GLOBWB 2 at 5 arc-minute resolution and compares them to a 30 arc-minute version. As discharge data are commonly used in hydrological model performance evaluation, the simulated river discharge of PCR-GLOBWB 2 is compared to in situ discharge observations from the Global Runoff Data Centre (GRDC, 2014).

The paper is organized as follows. Section 2 provides a global description of PCR-GLOBWB 2, including its model structure and the new components and functionalities that have been added since PCR-GLOBWB 1. In section 3 the global application of PCR-GLOBWB 2 is demonstrated and the results from a 58-year simulation (1958-2015) are evaluated against observations of discharge, total water storage and reported withdrawal data. Section 4 summarizes and concludes this paper and discusses possible future developments. Section 5 provides information about availability of the model code and the underlying data.

[1] Note that Wada et al. (2016) made a preliminary version of the model that operates at 6 arc-minutes.

2. PCR-GLOBWB 2 – Model description

2.1 General overview

PCR-GLOBWB 2 is a state-of-the-art grid-based global hydrology and water resources model. It is a component-based model implementation in Python using open source PCRaster Python routines (Karssenberg et al., 2010, http://pcraster.geo.uu.nl/). The code is distributed through Github. The computational grid covers all continents except Greenland and Antarctica. Currently two versions are available: one with a spatial resolution of 5 arc-minutes in latitude and longitude and one with a coarser resolution of 30 arc-minutes. Typical time steps for hydrology and water use are one-day while sub-daily time stepping is used for hydrodynamic river routing. For all dynamic processes involved, PCR-GLOWB 2 uses a time-explicit scheme. For each grid cell and each time step, PCR-GLOBWB 2 simulates moisture storage in two vertically stacked upper soil layers (S_1+S_2 in Figure 1), as well as the water exchange between the soil, the atmosphere and the underlying groundwater reservoir (S_3 in Figure 1). The exchange with the atmosphere comprises of precipitation, evaporation from soils, open water, snow and soils and plant transpiration, while the model also simulates snow accumulation and snowmelt. Sub-grid variability of land use, soils and topography is included and influences the schemes for runoff-infiltration partitioning, interflow, groundwater recharge (from S_2 to S_3) and capillary rise (from S_3 to S_2). Runoff, generated by snowmelt, surface runoff, interflow and baseflow, is routed across the river network to the ocean or endorheic lakes and wetlands. Routing can either be simple accumulation, simplified dynamic routing using a method of characteristics, or kinematic wave routing. In case the kinematic wave routing is used, it is also possible to use a (simplified) floodplain inundation scheme and to simulate the surface water temperature.

PCR-GLOBWB 2 includes a simple reservoir operation scheme that is applied to over roughly 6000 manmade reservoirs from the GranD database (Lehner et al., 2011), which are progressively introduced according to their construction year. Human water use is fully integrated within the hydrological model, meaning that at each time step: 1) water demands are estimated for irrigation, livestock, industry and households, 2) these demands are translated into actual withdrawals from groundwater, surface water (rivers, lakes and reservoirs) and desalinization, subject to availability of these resources and maximum groundwater pumping capacity in place, 3) consumptive water use and return flows are calculated per sector.

As an option PCR-GLOBWB 2 can be partially or fully coupled to a two-layer global groundwater model based on MODFLOW (de Graaf et al, 2017). Recent work (Hoch et al., 2017a,b) also includes coupling PCR-GLOBWB 2 to either Delft3D Flexible Mesh (Kernkamp et al., 2011) or LISFLOOD-FP (Bates et al., 2010) which are model codes that can be used to solve the 1D-2D shallow water equations (or approximations thereof) for detailed inundation studies.

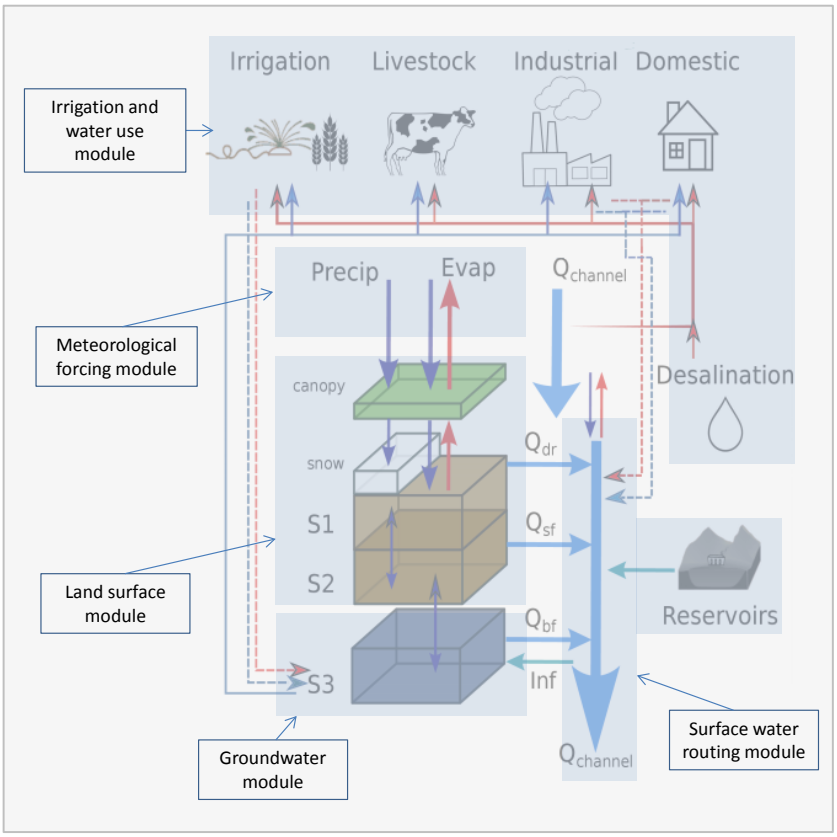

Figure 1. Schematic overview of a PCR-GLOBWB 2 cell and its modelled states and fluxes. S_1, S_2 (soil moisture storage), S_3 (groundwater storage), Q_{dr} (surface runoff – from rainfall and snowmelt), Q_{sf} (interflow or stormflow), Q_{bf} (baseflow or groundwater discharge), Inf *(riverbed infiltration from to groundwater). The thin red lines indicate surface water withdrawal, the thin blue lines groundwater abstraction, the thin red dashed lines return flows from surface water use and the thin dashed blue lines return flows from groundwater use surface. For each sector: withdrawal - return flow = consumption. Water consumption adds to total evaporation. In the figure, the five modules that make up PCR-GLOBWB 2 is portrayed on the model components.*

2.2 Model structure and flexibility

PCR-GLOBWB 2 has a flexible modular structure (Figure 1). The modular structure of PCR-GLOBWB 2, both in terms of model concepts and implementation (separate modules are called from a main program), makes it easy to modify or replace components according to specific objectives of the model application, to introduce new modules or components within the modelling system and to couple it to existing codes.

There are currently five main hydrological modules in PCR-GLOBWB 2 as illustrated in Figure 1 and briefly described in Section 2.3: Meteorological forcing, Land surface, Groundwater, Surface water routing, Irrigation and water use. For an extensive description of the underlying equations and methods used in each of these modules we refer to the following sources:

- Meteorological forcing module: van Beek (2008, http://vanbeek.geo.uu.nl/suppinfo/vanbeek2008.pdf)
- Land surface module, groundwater module and surface water routing module: van Beek and Bierkens (2009, http://vanbeek.geo.uu.nl/suppinfo/vanbeekbierkens2009.pdf), van Beek et al. (2011, http://dx.doi.org/10.1029/2010WR009791)
- Irrigation and water use module:
    - Calculation of water demand: Wada et al., (2014, https://doi.org/10.5194/esd-5-15-2014)
    - Calculation of water withdrawal, consumption and return flows: de Graaf et al. (2014, https://doi.org/10.1016/j.advwatres.2013.12.002), Wada et al. (2014, https://doi.org/10.5194/esd-5-15-2014), Erkens and Sutanudjaja (2015, https://doi.org/10.5194/piahs-372-83-2015)

Furthermore: for details about coupling to MOFLOW we refer to:

- One-way coupling: Sutanudjaja et al. (2011, https://doi.org/10.5194/hess-15-2913-2011), de Graaf et al. (2017, https://doi.org/10.1016/j.advwatres.2017.01.011)
- Two-way coupling: Sutanudjaja et al. (2014, http://dx.doi.org/10.1002/2013WR013807)

2.3 Description of the modules

Hereafter, we briefly describe the main features of the five modules. Additionally, a (non-exhaustive) list of the model state and flux variables is provided in Table A1, whereas Table A2 lists the model inputs and parameters, including their sources.

2.3.1 Meteorological forcing module

Meteorological forcing of PCR-GLOBWB 2 uses time series of spatial fields of precipitation, temperature and reference evaporation. Reference potential evaporation can be prescribed or calculated within the model, and is used in the land surface module to calculate land-cover specific potential evaporation based on crop factors of the various land cover types according to the FAO guidelines (Allen et al., 1998). There are two options for calculating reference potential evaporation: 1) using Hamon (1963) in case only daily mean temperature is available, 2) using Penman-Monteith following the FAO guidelines (Allen et al., 1998) if net radiation, wind speed and vapour pressure deficit are additionally available. See van Beek et al. (2008) for details. The resulting land-cover specific potential evaporation is subsequently used to compute the actual evaporation for different land cover types in each cell. Apart from the calculation of evaporation, temperature is also used to partition precipitation into snow and rain and to drive snowmelt.

2.3.2. Land surface module

This core module of PCR-GLOBWB 2 covers the land-atmosphere exchange, the vertical flow between soil compartments and the eventual groundwater recharge, snow and interception storage and the runoff generation mechanisms. These processes are simulated over a number of land cover types and aggregated proportionally based on land cover fractions within a model cell. Users can specify their own land cover classification and introduce their own land cover parameterization. The number of land cover types is configurable. The standard parameterization of PCR-GLOBWB 2 carries four land cover types consisting of tall natural vegetation, short natural vegetation, non-paddy irrigated crops, and paddy irrigated crops (i.e. wet rice). There is also a parameterization set for six land cover types (Bosmans et al., 2017), albeit still at 30 arc minute resolution only, that includes distinct types for pasture and rain-fed crops. For the standard four land cover parameterization of PCR-GLOBWB, applied in this paper, the land cover types of pasture and rain-fed crops are integrated into the short natural vegetation type.

For each land cover type, separate soil conditions can be specified. It should be noted that the soil and vegetation conditions are in any case fully spatially distributed. Thus, vegetation properties (e.g., crop factor, Leaf Area Index) and soil properties (depth, saturated hydraulic conductivity, etc.) vary not only between land cover types, but may also vary from cell-to-cell (e.g., per climate zone). In the standard parameterization vegetation properties vary over the year using a monthly climatology of phenology and crop calendars (i.e. for the crop factor and LAI). The application of irrigation water for paddy and non-paddy irrigation is done by the irrigation and water use module. It is based on the FAO guidelines of Allen et al. (1998) and is dependent on the actual soil water storage (S_1, S_2) or paddy-open water storages. All fluxes, from and to the land surface module in Figure 1, are thus calculated separately per land cover type. The resulting vertical fluxes for each land cover type are: interception evaporation, bare soil evaporation, snow sublimation, vegetation-specific transpiration. In the soil column, vertical fluxes are driven by degrees of saturation of soil layers and interact with the underlying groundwater store, S_3 (see e.g. van Beek and Bierkens, 2009; Sutanudjaja et al., 2011; Sutanudjaja 2012 for detailed explanation). Surface

runoff (Q_{dr}, from precipitation and snowmelt) consists of infiltration excess runoff and saturation excess runoff following a sub-grid approach that mimics variable source areas, i.e. the improved Arno Scheme (Todini, 1996, Hagemann and Gates, 2003). Interflow or stormflow (Q_{sf}), mostly occurring in regolith soils on hillslopes, is also handled with a sub-grid approach based on a runoff parameterization by Sloan and Moore (1984). All fluxes are computed per land cover type and balanced with the available storage to arrive at the net flux that is used to update the storages for the next time step. Also, to report the overall fluxes per cell, and to pass these to other modules, the land cover specific fluxes are subsequently averaged (weighted by land cover type fractions).

For the standard parameterization of the land surface module the following data sets are combined (see Table A2): the cell fractions of various non-irrigation land cover types are based on the map of Global Land Cover Characteristics Data (GLCC) Base Version 2.0 (Loveland et al., 2000) with the land cover classification following Olson (1994a, b) and the parameter sets from Hagemann et al. (1999) and Hagemann (2002). Irrigation land cover types (i.e. paddy and non-paddy), including their crop calendars and growing season lengths, are parameterized based on the data set of MIRCA2000 (Portmann et al., 2010) and the Global Crop Water Model of Siebert and Döll (2010). We refer to van Beek et al. (2011) for detailed descriptions.

2.3.3. Groundwater module

The groundwater module calculates groundwater storage dynamics subject to recharge and capillary rise (calculated by the land surface module), groundwater discharge (Q_{bf}, in case of a positive groundwater storage) and riverbed infiltration (Inf). Groundwater discharge (assumed the same as groundwater baseflow here) depends on a linear storage-outflow relationship ($Q_{bf} = S_3/J$) where the proportionality constant J is calculated following drainage theory of Kraijenhoff-van de Leur (1958) based on drainage network density and aquifer properties. Riverbed infiltration occurs only in case Q_{bf} becomes 0 by groundwater withdrawal. Under persistent groundwater withdrawal (calculated with the Irrigation and Water use module) that is larger than the sum of recharge and riverbed infiltration, the groundwater storage S_3 is allowed to become negative. In this case, the part of the withdrawn groundwater in excess of the input (recharge and riverbed infiltration) is seen as non-renewable groundwater withdrawal leading to groundwater depletion (permanent loss of groundwater from storage). In case withdrawal becomes smaller than the input, the remaining input is used to first fill the negative storage to zero, before baseflow Q_{bf} commences again. As an alternative, it is also possible to limit the maximum volume of non-renewable groundwater that can be extracted. .

It is possible to use a full-fledged groundwater flow model based on MODFLOW (Harbaugh et al., 2000) coupled to PCR-GLOBWB 2 in order to calculate groundwater heads and flow paths. This can be done as a one-way coupling where PCR-GLOWB 2 is first run with the standard groundwater module (reservoir S_3 with only vertical fluxes) to yield time series of net groundwater recharge (recharge – capillary rise) and surface water levels. These fluxes/inputs are subsequently used to force the groundwater flow model (see e.g. Sutanudjaja et al., 2011, de Graaf et al., 2017). Another possibility is to use a two-way coupling where the groundwater module of PCR-GLOBWB 2 is replaced by the groundwater flow model. In this case, at each time

step fluxes are exchanged between the groundwater model and the land surface module, and the groundwater model and the surface water routing module (Sutanudjaja et al. 2014).

2.3.4 Surface water routing module

Following an 8-point steepest gradient algorithm across the terrain surface (local drainage direction or LDD), all cells of the modelled domain are connected to a strictly convergent drainage network that together makes up the river basins and sub-basins of the model domain. The lowermost cell is either connected to the ocean or to an endorheic basin. Per cell, the sum of the three daily runoff fluxes (Figure 1) is aggregated and routed along the drainage network until passing the lowermost cell and being removed from the model. Routing can be done in three ways of increasing complexity: 1) simple accumulation of the fluxes over the drainage network; 2) a travel-time characteristic solution (Karssenberg et al., 2007), and 3) the kinematic wave solution.

The first method is typically aggregated over longer time steps (e.g. month or year) that are larger than the travel times of water along the longest river length. The second routing method includes an estimation of cell flow velocity based on average discharge from the last 5 years and Manning's equation, which assumes the energy slope to be equal to the bed slope. This estimated velocity is used to move the volume of water in the channel of a cell the corresponding distance within one daily time step along the drainage network. This method works reasonably well for relatively steep rivers in humid climates where the friction slope is close to the bed slope and the rivers are equally filled with water throughout the year. The third method is the kinematic wave approximation of the Saint Venant equations with flow described by Manning's equation, Also, here, it is assumed that friction slope and bed slope are equal, which makes it valid for rivers without backwater effects. The kinematic wave is solved using a time-explicit variable sub-time stepping scheme based on the minimum Courant number. Of these methods, the kinematic wave solution simulates the propagation of the flood wave more realistically while the others provide an expedient means to approximate discharge over longer periods.

Using the kinematic wave method, it is possible to model floodplain inundation which occurs if the discharge exceeds the bankfull capacity of a channel. The excess discharge volume is spread over the entire cell from the lowest part of the cell (based on a higher resolution sub-grid DEM) yielding a flooded area with an approximated flood depth. In case of flooding, the simulated river flow is impacted by adjusting the wetted area and wetted perimeter and calculating a weighted Manning coefficient from the individual Manning coefficients of the floodplains and the channel.

Lakes and reservoirs are part of the drainage network. Lakes and reservoirs can extend over multiple cells, in which case the storage is subdivided by area such as to ensure that lake and reservoir levels are the same across their extent. The active storage of lakes and the actual storage of reservoirs are dynamically updated, for the lake outflow a standard storage-outflow relationship based on a rectangular cross-section over a broad-crested weir (Bos, 1989) is used, while reservoirs follow a release strategy. This strategy is, by default, aimed at passing the average discharge, while maintaining levels between a minimum and maximum storage (Wada et al., 2014), but

more elaborate strategies that take account of downstream water demand are possible (e.g. van Beek et al., 2011). Lakes and reservoir areas change based on global volume-area relationships. All surface water areas, which can be classified into several water types, river channels, inundated floodplains, lakes and reservoirs, are subject to open water evaporation calculated from reference potential evaporation multiplied with factors depending on water types and depths. Moreover, surface waters are subject to surface water withdrawal calculated with the Irrigation and Water Use module.

If the kinematic wave approach is used, it can be also augmented with an energy routing scheme to simulate surface water temperature (van Beek et al., 2012). Finally, it should be noted that it is possible to run the routing routine from PCR-GLOBWB 2 as a stand-alone routine, which allows it to be fed with the specific discharge from other land surface models.

The routing methods that are available in PCR-GLOBWB 2 will yield significant errors for wide lowland rivers where backwater effects are important. In this case, it is possible to replace the surface water module for part of the modelling domain with hydrodynamic models solving the shallow water equations (Hoch et al., 2017a). Hoch et al. (2017b) developed a generic coupler for this purpose that enables coupling to multiple hydrodynamic modelling codes (https://doi.org/10.5281/zenodo.597107).

Although any data set can be used to define the drainage network and locate the lakes and reservoirs, the standard parameterization of PCR-GLOBWB 2 that runs globally uses the drainage network derived from the high resolution 30 arc-sec HydroSHEDS (Lehner et al., 2008) combined with 30 arc-sec GTOPO30 (Gesch et al., 1999) and 1 km Hydro1k (Verdin and Greenlee, 1996, USGS EROS Data Center, 2006), lakes taken from GLWD (Lehner and Döll, 2004) and reservoirs obtained from GranD (Lehner et al., 2011).

2.3.5 Irrigation and water use module

In PCR-GLOWB 1 water demand was calculated separately from the hydrology and water availability calculated as a post-processing step by subtracting upstream demand (Wada et al., 2011a,b). In PCR-GLOBWB 2 water use (withdrawal and consumption) is fully integrated. Hereafter, the main features of the irrigation and water use module are described in the following order: water demand, water withdrawal, water consumption and return flows.

Water demand

Irrigation water demand is calculated based on the crop composition (which changes per month and includes multi-cropping) and the irrigated area per cell. As stated above, these are obtained from MIRCA2000 (Portmann et al., 2010) and the Global Crop Water Model (Siebert and Döll, 2010). In the standard PCR-GLOBWB 2 parameterization the irrigated areas change over time. In want of detailed data, fractions of paddy and non-paddy irrigation, as well as the crop composition per month stay fixed (as obtained from MIRCA2000), while the total irrigated area per cell changes over time and is based on the FAOSTAT (FAO, 2012) reported irrigated areas. Irrigation water demand is computed using the FAO guidelines (Doorenbos and Pruit, 1977, Allen et al., 1998): in case of non-paddy irrigation, water is applied whenever soil moisture falls below a pre-set value and then the soil column is replenished up to field capacity. In case of paddy irrigation, the water level is kept at a water depth of 5 cm above the surface until the late crop development stage (~ 20 days) before the harvest. After that, no irrigation is applied anymore such that the water level is allowed to drop to zero under infiltration and evaporation (Wada et al., 2014). The net irrigation demand is augmented to account for limited irrigation efficiency and losses. In order to obtain irrigation water demand including losses, i.e. gross irrigation demand, net irrigation water demand is multiplied with $(1 + f_I)$, with f_I a country-specific loss factor obtained from Rohwer et al. (2007).

Non-irrigation water demand covers three sectors, industry, households and livestock. For each of these sectors, the gross demand and net demand are prescribed to the model. The calculation of net non-irrigation water demand, which varies with time, follows methods developed by Wada et al (2014). We refer to Wada et al. (2014) for an extensive description. Trends in water demand are prescribed on an annual basis as a function of population, electricity demand and gross domestic product (GDP) per capita. In addition, domestic water demand exhibits a seasonal variation on the basis of temperature. Domestic and industrial gross water demand is calculated from net water demand using a country-specific recycling ratio *RC* (based on development stage or GDP per capita and additionally access to domestic water demand): gross = net/(1-*RC*). This takes into account that much of the domestic and industrial water is not consumed but returned as surface water. For livestock, the return flow is assumed to be zero, meaning all water is consumed.

Water withdrawal

The water withdrawal estimation is based on the work by de Graaf et al. (2014) and Wada et al. (2014). In PCR-GLOBWB 2 water withdrawal is set equal to gross water demand (summed over all the sectors) unless sufficient water is not available. In that case, water withdrawal is scaled down to the available water and then allocated proportionally to gross water demand per sector. Thus, no allocation preference is available in the standard parameterization of PCR-GLOBWB 2.

Water can be abstracted from three sources: surface water, groundwater (fossil and non-fossil) and desalinated water. The latter is prescribed (Wada et al., 2011a), while the fractions of the other two sources are determined as a function of their relative abundance. Groundwater and surface water availability are determined based on two-year running means of groundwater recharge and river discharge respectively, thus keeping track of the prevalence of local resources and their temporal change (de Graaf et al., 2014). These fractions determine on a monthly basis from which source water is abstracted. Surface water withdrawal is ceased if river discharge falls below 10% of the long-term average yearly discharge under naturalized flow conditions (determined by running the model without withdrawal). If, for some reason, the surface water amount is insufficient, the model falls back on groundwater to meet the resulting gap. Groundwater is first abstracted from the renewable groundwater storage, and if this is not present, non-renewable groundwater is abstracted. The amount of groundwater that can be abstracted is, however, capped by the groundwater pumping capacity which is based on data by IGRAC GGIS database. The described dynamic allocation scheme is not always in line with local preferences or the infrastructure. However, there is a possibility to use fractions of groundwater and surface water withdrawal reported in the literature. For urban areas, we rely on the data set of McDonald et al. (2014) that states whether a surface water distribution infrastructure is available. If this is the case, industrial and domestic water withdrawals are mainly taken from surface water before abstracting groundwater. If surface water infrastructure is limited, groundwater source is prioritized (see e.g. Erkens and Sutanudjaja, 2015). For urban areas that are not in the McDonald (2014) data set, we give preference to the dynamic allocation scheme. For irrigation, we use the ratios supplied by Siebert et al. (2010) in regions where they are said to be reliable. In regions where they are not fully reliable, we take the average ratio provided by Siebert et al. (2010) and the one provided by the dynamic allocation scheme. For regions where the data of Siebert (2010) are not reliable (i.e., extrapolated data), we give preference to the dynamic allocation scheme.

Moreover, we cannot assume that all the water demand is supplied from surface water and groundwater resources in the same cell. Ideally, data about local water redistribution networks and inter-basin transfers should be used to define surface water and groundwater service areas. Unfortunately, this information is not available at the global scale. Therefore, in our current parameterization of PCR-GLOBWB 2, we pool water availability of desalinated and surface water over zones of approximately 1 arc-degree by 1 arc-degree size that are truncated by country borders if applicable. For groundwater, 0.5 arc-degree zones are used. The downside of the current scheme is that a cell does not always have access to its nearest water resource if this lies outside its prescribed service area.

Water consumption and return flows

In case of irrigation, all the withdrawn water is applied to the soil (non-paddy) or the water level on the field (paddy). Part of that water is lost by transpiration and part by soil and open water evaporation. Transpiration and evaporation together make up the irrigation water consumption. The remaining part of irrigated water is lost by percolation and contributes to groundwater recharge as return flow. Irrigation efficiency (not including conveyance losses) could also be calculated after the fact by the difference between withdrawal and transpiration. In case of domestic and industrial water use, water consumption depends on the recycling ratio RC and equals withdrawal×(1-RC), while withdrawal×RC constitutes return flow. All return flow is added to the surface water. For livestock, the consumption is set equal to the withdrawal and no return flow is assumed.

438 **2.4 Model code**

439

440 The original PCR-GLOBWB version 1 (van Beek et al., 2011) was written in the PCRaster scripting language.
441 PCRaster (Wesseling et al., 1996) is a high-level programming language that started as a dynamic raster-based
442 Geographical Information System (GIS) and is tailored to spatiotemporal modelling for environmental and earth
443 science applications. The generic nature of PCRaster with its many pre-existing built-in hydrological functions and
444 its syntax that reads like pseudo-code, generally results in concise model codes, short development times and
445 limited programming errors. Karssenberg et al. (2010) developed a PCRaster Python package such that PCRaster
446 functions, implemented in C++, can also be called via Python (http://www.python.org/). Using PCRaster Python
447 makes it possible for students and beginner modellers to contribute to the model quickly, while it allows experts to
448 be more productive and focus on the science rather than on the programming language syntax. Realising the
449 aforementioned advantages, PCR-GLOBWB, particularly starting from this version 2, has been rewritten in the
450 Python scripting language.

451

452 To allow for exchanges of model components and, therefore, evaluate different model configurations, a
453 component-based development approach (e.g Argent, 2004; Castronova and Goodall, 2010) was followed while
454 developing the PCR-GLOBWB 2 model code. Each of the PCR-GLOBWB scientific modules described in section
455 2.3 is implemented in a separate Python class that needs to implement initialization and update methods. The latter
456 designates changes of states and fluxes per time step. Each of module is initialized and executed by iteratively
457 calling the update method via a main model script.

458

459 To run the model a so-called initialization file or configuration file is used (with extension .ini). In this file the
460 following aspects are defined: the spatial and temporal domain, the time step, the settings of the different modules
461 (e.g. which surface water routing, human water use or not etc.) and the locations and names of the parameter files
462 and forcing files. PCR-GLOBWB 2 uses NetCDF files for most input and all output, thus making it easier to
463 exchange data with other scientists and use existing tools to analyse its output.

464

465 PCR-GLOBWB 2 generally runs best under Linux. In order to run PCR-GLOBWB the following additional
466 software needs to be installed: PCRaster version 4, Python versions 2.7 with Python packages numPy and
467 netCDF4 and gdal version 1.8 or higher.

468

2.5 Differences between PCR-GLOBWB 1 and 2

PCR-GLOBWB 2 has the following new capabilities compared to PCR-GLOBWB 1 (cf. van Beek et al., 2011, Wada et al, 2011):

- the model was completely rewritten in PCRaster Python and now has a modular structure,
- the inputs and outputs are in the form of NetCDF files and output can be reported for daily monthly and yearly time steps,
- parameterizations are available at 30 arc-minute and 5 arc-minute resolutions,
- water use (demand, withdrawal, consumption and return flow) is fully integrated,
- distinction is made between paddy and non-paddy irrigation and irrigation follows FAO guidelines,
- three different options for surface water routing are available and a surface water temperature module is fully integrated with the routing scheme,
- it is possible to run surface water routines separately with specific discharge from other sources (e.g. other land surface models),
- PCR-GLOBWB 2 can be coupled to a two-layer transient groundwater model (Sutanudjaja et al., 2014, de Graaf et al., 2017) and to the hydrodynamic models Delft3D Flexible Mesh (Kernkamp et al., 2011) or LISFLOOD-FP (Bates et al., 2010, see Hoch et al., 2017b).

3. Model demonstration and evaluation

To test and evaluate the performance of PCR-GLOBWB 2, we ran the model at both 30 arc-minute and 5 arc-minute resolution over the period 1958-2015. We compared the results of both simulations with discharge data from the Global Runoff Data Centre (GRDC, 2014), with total basin water storage estimates from GRACE (Gravity Recovery and Climate Experiment, Wiese, 2015) and with water withdrawal data from the FAO AQUASTAT database (FAO, 2016).

3.1 Model run setup

3.1.1 Parameterization

We used the standard parameterization (parameters, forcing and their sources in Table A2) of PCR-GLOBWB 2 at 30 arc-minute and 5 arc-minute spatial resolutions to simulate global hydrology at daily resolution over 1958-2015. Outputs were reported as monthly averages. The parameterization was mostly unchanged from that given in van Beek and Bierkens (2009), but newer datasets were used if available, such as the GRAND (Lehner et al., 2011) dataset for reservoirs and MIRCA (Portmann et al., 2010) for crop areas. We stress that no calibration was performed. We ran the model with human water use options turned on and used the travel-time characteristic solution routing option.

3.1.2 Forcing

The forcing data set is based on time series of monthly precipitation, temperature and reference evaporation from the CRU TS 3.2 data set of Harris et al. (2014) downscaled to daily values with ERA40 (1958-1978, Uppala et al., 2005) and ERA-Interim (1979-2015, Dee et al., 2011). CRU is specified at 30 arc-minute spatial resolution and directly usable. We used ERA40 and ERA-I results that had been resampled by ECMWFs resampling scheme from their original resolutions (~1.2º and ~0.7º) to 30 arc-minutes first. Here, resampling means a form of spatial downscaling whereby the values of the larger ERA40 and ERA-I grid cells are assigned to the cell centers and then spatially interpolated onto 30 arc-minute grids. Precipitation was temporally downscaled by first applying a threshold of 0.1 mm/day to the ERA daily time series to estimate the number of rain days for ERA. The amount of rainfall below this threshold was proportionally allocated to the rain days. Next, the daily rainfall totals were scaled in order to reproduce the CRU monthly precipitation total using multiplicative scaling. Equally, monthly reference potential evaporation, computed with Penman-Monteith from the CRU data set, was scaled using multiplicative scaling and downscaled to daily data proportional to Hamon (1967) evaporation calculated from daily ERA temperatures. We elected not to calculate Penman-Monteith reference evaporation directly from the ERA40 and ERA-I data, in order to avoid the large calculation times needed to process the required meteorological values. For the air temperature, an additive scaling factor was used. To better simulate snow-dynamics for the 5arc-minute model, the temperature values from CRU were further spatially downscaled to 5 arc-minutes using a temperature lapse-rate derived from the higher-resolution CRU CL 2.0 climatology (New et al., 2002). For areas where the number of stations underlying the CRU data set was found to be small, preference was given to using directly the meteorological data from ERA. The method used to create the forcing data set is described more extensively in van Beek (2008).

3.1.3 Spin-up

The large groundwater response times for certain regions (e.g. Niger and Amazon) requires substantial spin-up for the groundwater volumes to be in equilibrium with the current climate. To reach this equilibrium, the model was spun-up using the average climatological forcing over the years 1958–2000 back-to-back for 150 years to reach a dynamic steady state. This spin-up was executed under naturalized condition which means no reservoirs and no human water use.

3.1.4 Computation time and parallelization

The models were run on Cartesius, the Dutch national supercomputer (https://userinfo.surfsara.nl/systems/cartesius). Without parallelization, the wall clock time for a one-year global simulation run of the 30 arc-minute model was about one hour. This entails that a one-year global simulation run with the 5 arc-minute model, might result in wall clock times of at least 36 hours. Hence, to speed-up computation, the 5 arc-minute model domain was divided into 53 groups of river basins such that it could be run as 53 separate processes. With this simple parallelization technique, the wall clock time for a one-year simulation run of the 5 arc-minute model reduced to about one hour again. Note that these computation times were obtained for simulations with the travel-time characteristic routing option. Calculation times would have been significantly longer if the kinematic wave routing had been used (e.g. about 6 hours for a one-year 5 arc-minutes global run including parallelization).

3.2 Data used for comparison

3.2.1 River discharge

We used discharge stations from GRDC (2014) to compare simulated discharge from PCR-GLOBWB 2 with monthly reported discharge. From all the globally available stations in the database, we selected a subset of stations using the following criteria: 1) allowing a not more than 15% difference in catchment area between PCR-GLOBWB 2 and the area reported with the GRDC discharge station, 2) not more than 1 cell distance between the station location and the nearby location of a river in PCR-GLOBWB 2, 3) at least 1 year of discharge data. This yielded 5363 stations for the 5 arc-minute simulation, 3910 stations for the 30 arc-minute simulation and 3597 stations fulfilling the criteria for both resolutions. The minimum, median and maximum catchment sizes for the GRDC stations at the 5 arc-minute resolution are respectively 29, 2730 and $4.68 \cdot 10^6 km^2$ and 31, 6560 and $4.68 \cdot 10^6 km^2$ at the 30 arc-minute resolution. As we jointly compared the performance of both simulations, we used the set of 3597 locations throughout. The average time series length of these stations is equal to 36 years.

3.2.2 Total water storage

We compared total water storage (TWS) as simulated by PCR-GLOBWB 2 with the TWS estimated from GRACE (Gravity Recovery and Climate Experiment) gravity anomalies. We used the GRACE JPL Mascon product PL-RL05M (Wiese, 2015, Watkins et al., 2015, Wiese et al., 2016). Scanlon et al. (2016) suggest that recent developments in mascon (mass concentration) solutions for GRACE have significantly increased the spatial localization and amplitude of recovered terrestrial TWS signals. They also claim that one of the advantages of using the mascon solutions relative to traditional SH (spherical harmonic) solutions is that it makes it much easier for non-geodesists to apply GRACE data to hydrologic problems. Note that although the data of PL-RL05M are represented on a 30 arc-minutes lat-lon grid, they represent the 3x3 arc-degree equal-area zones, which is the actual resolution of JPL-RL05M. We compared trends on

a pixel-by-pixel basis. Given the coarse resolution of GRACE products of about 300 km by 300 km we compared correlations only for major river basins with an area of 900,000 km^2 and up.

3.2.3 Water withdrawal

The water withdrawal for a large number of countries is taken from FAO's AQUASTAT database (FAO, 2016). This data is on average reported in every 5 years. We compared simulated water withdrawal per sector and per water source (surface water and groundwater) with reported values per country and per reporting period, whenever available.

3.3 The global water balance simulated at 30 and 5 arc-minutes

We calculated the main global water balance components from the 30 arc-minute and 5 arc-minute simulations over the period 2000-2015. The results in Table 1 show that there are some differences between the two model runs, but values are in the same order of magnitude. The small difference in precipitation is due to the fact that the area of the land cells is slightly different at the two resolutions. Differences in evaporation and runoff show that the runoff and evaporation parameterization of PCR-GLOBWB 2 is not entirely scale-consistent. Differences in evaporation may also be causing the differences in irrigation water demand which in turn may explain the differences in water withdrawal. Recently, Samaniego et al. (2017) applied their multiscale parameter regionalization (creating spatially variable parameter fields) technique (MPR) to PCR-GLOBWB 2 for the Rhine basin, showing that parameterizations that yield the same hydrological fluxes at different resolutions are possible. However, a global application of this method to all PCR-GLOWB 2 parameters is not possible yet. Nonetheless, when comparing the results of both model runs with data reported in the literature, it shows that the global water balance components are similar to recent assessments (e.g. by Rodell et al., 2015) and groundwater withdrawal and total withdrawal estimates match those of previous studies (see Table 2).

From Table 1, it can also be seen that there is a negative change in total terrestrial water storage in both model runs. Table 1 shows that this can only be partly explained by groundwater depletion, which is localized to certain regions (see also Sect. 3.4.2). Further analysis shows that this change can also be attributed to the trends in precipitation forcing used, particularly over the tropics.

Table 1. Global Water balance components and human water withdrawal (in km^3/year and mm/year) over the period 2000-2015 as obtained from the 30 arc-minutes and the 5 arc-minute simulations. The numbers are shown to high significance to show the water balance closure. This does not mean that we pretend to know e.g. global discharge with a km^3 accuracy (actual accuracy of the large fluxes is more in the order of 10^3 km^3)

		30 arc-min		5 arc-min	
		km^3/year	mm/year	km^3/year	mm/year
Global water balance	Precipitation	107452	808	107495	811
	Desalinated water use	3	0.02	2	0.01
	Runoff	42393	319	43978	332
	Evaporation*	65754	494	63974	483
	Change in total water storage	-693	-5	-455	-3
Groundwater budget	Groundwater recharge	27756	209	25521	193
	Groundwater withdrawal	737	6	632	5
	Non-renewable groundwater withdrawal (groundwater depletion)	173	1	171	1
	Renewable groundwater withdrawal	564	4	460	3
Withdrawal by sector	Agricultural water withdrawal (irrigation + livestock)	2735	21	2309	17
	Domestic water withdrawal	380	3	314	2
	Industrial water withdrawal	798	6	707	5
Withdrawal by source	Total water withdrawal	3912	29	3330	25
	Surface water withdrawal	3172	24	2697	20
	Desalinated water use	3	0.02	2	0.01
	Groundwater withdrawal	737	6	632	5

* Includes consumptive water use for livestock, domestic and industrial sectors

Table 2. Groundwater withdrawal and total water withdrawal as compared to other studies (in km^3/year)

	Source	Year	Value (km^3/year)
Groundwater withdrawal	Wada et al. (2010) (from the IGRAC database)	2000	734 (±87)
	Döll et al. (2012)	1998-2002	571
	Döll et al. (2014) (their Table 2).	2003-2009	690-888
	Döll et al. (2014) (their Table 6).	2000-2009	665
	Pokhrel et al. (2015)	1998-2002	570 (±61)
	Hanasaki et al. (2018)	2000	789 (±30)
	This study (5 arc-minutes)	2000-2015	632
Total water withdrawal	Vörösmarty et al. (2005)	1995-2000	3560
	Oki and Kanae (2006)	contemporary	3800
	Döll et al. (2012)	1998-2002	4340
	Döll et al. (2014) (their Table 2)	2003-2009	3000-3700
	FAO (2016)	2010	3583
	Hanasaki et al. (2018)	2000	3628 (±75)
	This study (5 arc-minutes)	2000-2015	3330

3.4 Evaluation of the 30 and 5 arc-minute simulations

3.4.1 Discharge

When evaluating the simulated discharge with discharge observations from GRDC, we used the monthly values and calculated three different measures. The first one is the correlation coefficient between monthly simulated and observed GRDC time series, which is a measure of reproducing correct timing of high and low discharge. A correlation coefficient of 1 indicates perfect timing. The second measure is the Kling-Gupta efficiency coefficient or KGE (Gupta et al., 2009) which equally measures bias, differences in amplitude and differences in timing between monthly simulated and observed GRDC time series. The KGE varies between 1 and minus infinity, where 1 means a perfect fit in terms of bias, amplitude and timing. The last metric is the anomaly correlation, i.e. the correlation between monthly time series after the seasonal signal (climatology) has been removed. This statistic measures the ability of the model to correctly simulate timing of seasonal and the inter-annual anomalies from the yearly climatology. This is to test if the model is able to capture the monthly scale and inter-annual anomalies in discharge (i.e. on the monthly scale) when the dominant seasonal trend is removed from observations and simulations. An anomaly correlation of 1 indicates perfect characterization of inter-annual anomalies and values below 0 indicate a lack thereof.

Figure 2 shows maps of the correlation coefficients for the GRDC stations considered and Figure 3 shows histograms of correlation and KGE values. Both figures show that the evaluation results of the 5 arc-minute simulation are generally better than those of the 30 arc-minute simulation. For the 30 arc-minute model, the number of catchments with KGE > 0, 0.3 and 0.6 are equal to 48%, 26% and 7% of the total catchments respectively. For the 5 arc-minute model, these values are respectively equal to 63%, 40% and 12% of the total catchments. Note that for both runs the standard parameterization was used. Possible explanations for the better performance of the 5 arc-minute run are: a better delineation of the shape of the basins, particularly the smaller ones, a better characterization of basin relief and the drainage network, more accurate sub-grid parameterization of soil and land cover due to a smaller scale-gap that needs to be overcome, better estimates of the basin storage and better snow dynamics due to the downscaling of temperature to 5 arc-minute resolution. The KGE values are less favourable than the correlation coefficients. This is mostly due to biases in runoff caused by incorrect meteorological forcing. It is difficult to exactly assess which of these factors are most important in determining the improvement. Inspecting the histograms of correlation and KGE (Figure 3) shows that the improvement is mostly apparent for the smaller sized catchments, which supports the notion that a better delineation of the catchments' shape, topography and drainage network could be the cause. However, disentangling these individual effects would require further study. To investigate the possible effects of better snow dynamics we classified the GRDC stations into stations below 1000 m altitude (above mean sea-level) and those above 1000 m. The GRDC stations above 1000 m are expected to experience precipitation falling as snow during periods of the year. The results in Figure 4 clearly show that the improvement is larger for the higher GRDC stations, This supports the explanation that better snow dynamics due to temperature lapsing in combination with a better resolved digital elevation model is partly responsible for the superior results at 5 arc-minutes. We

also investigated if improvements were notably different between climate zones, by separately calculating KGEs for GRDC stations in the Köppen-Geiger zones A (Tropical), B (Desert), C (Temperate) and D (Continental). The results (not shown) show that the improvement is equally visible for climate zones A, B and C and less so for D (continental). Without further analysis this is difficult to explain. Note however that the continental climate zone is somewhat under-represented in the GRDC dataset due to the low measurement densities over Russia, although it is well represented in the U.S. So, it may be that the global improvements shown in Figure 3 are somewhat positively biased.

The maps of correlations (Figure 2) show the best results in Europe and North America where the meteorological forcing is generally more accurate as a result of more data used in the re-analysis products and higher station availability in the CRU data set. Also, monsoon-dominated basins are well simulated due to the strong seasonal nature of both forcing and related discharge. The improvement of the 5 arc-minute simulation over the 30 arc-minute simulation in Europe is mostly seen in the Alps and the Norwegian mountains. This reflects the fact that topography and thus snow dynamics is better represented at higher resolution as shown in Figure 4. The least accurate results are obtained for some of the African rivers, in particular the Niger where the groundwater recession coefficients are probably over-estimated and inland delta evaporation is under-estimated, for some rivers in the Rocky Mountains, which may be the result of errors in snow dynamics and for continental Eastern Europe, which is most likely explained by an over-estimation of the groundwater recession constants.

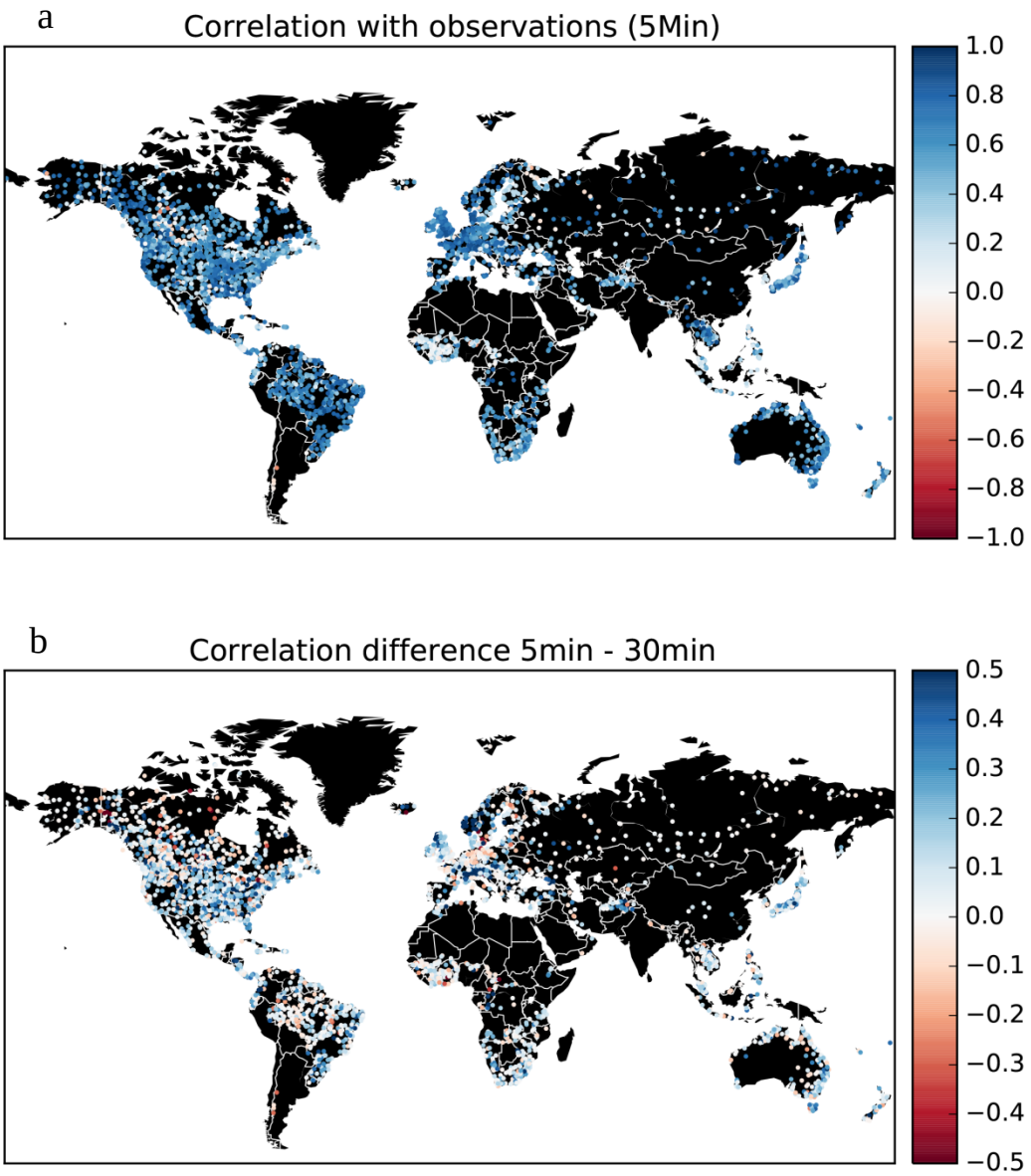

687

688 *Figure 2. Maps of correlation between simulated and observed discharge time series for 3597 GRDC discharge*
689 *stations; a. results for the 5 arc-minutes simulation; b. difference between results for 5 arc-minutes and 30 arc-*
690 *minutes simulation.*

691

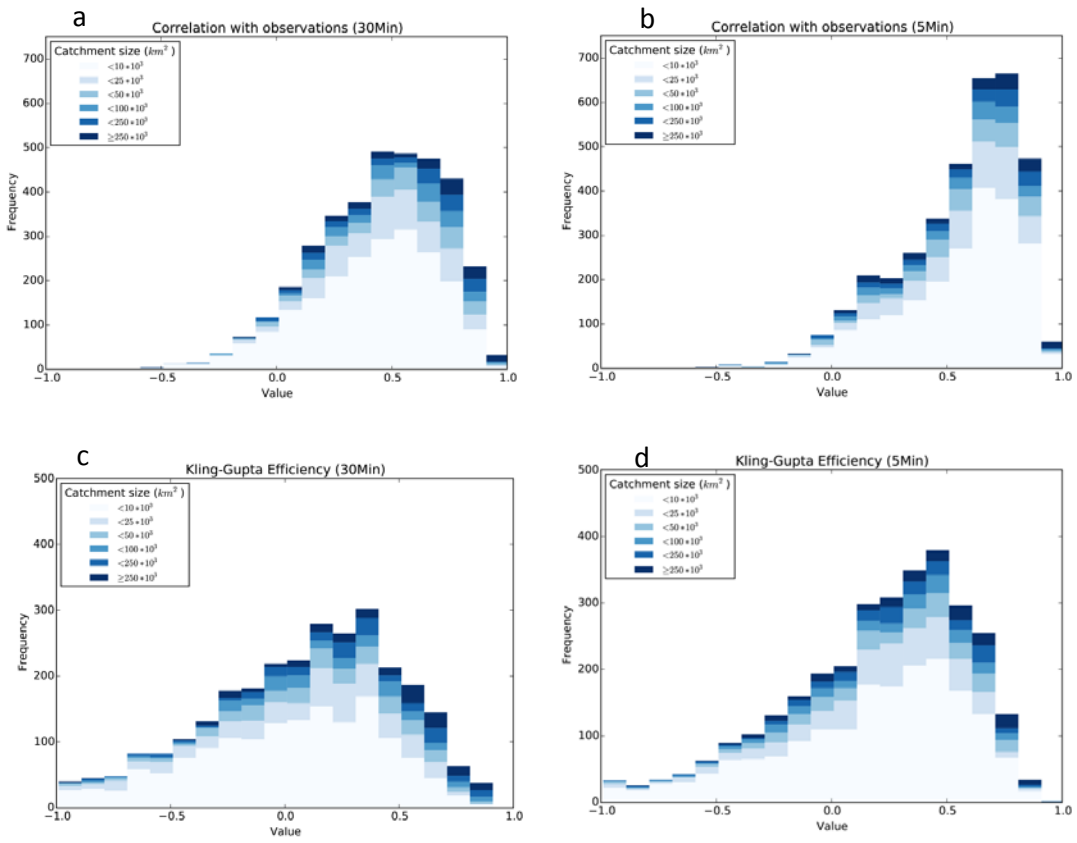

Figure 3. Histograms of evaluation statistics showing the correlation and Kling-Gupta efficiency (KGE) values for the simulated discharge for the 30 arc-minutes and the 5 arc-minute simulations based on 3597 GRDC discharge stations, a. correlation 30 arc-minute simulation, b. correlation 5 arc-minute simulation, c. KGE 30 arc-minute simulation, d. KGE 5 arc-minute simulation, note: the percentage catchments with KGE < -1 are 21% and 12% for 30 and 5 arc-minutes respectively.

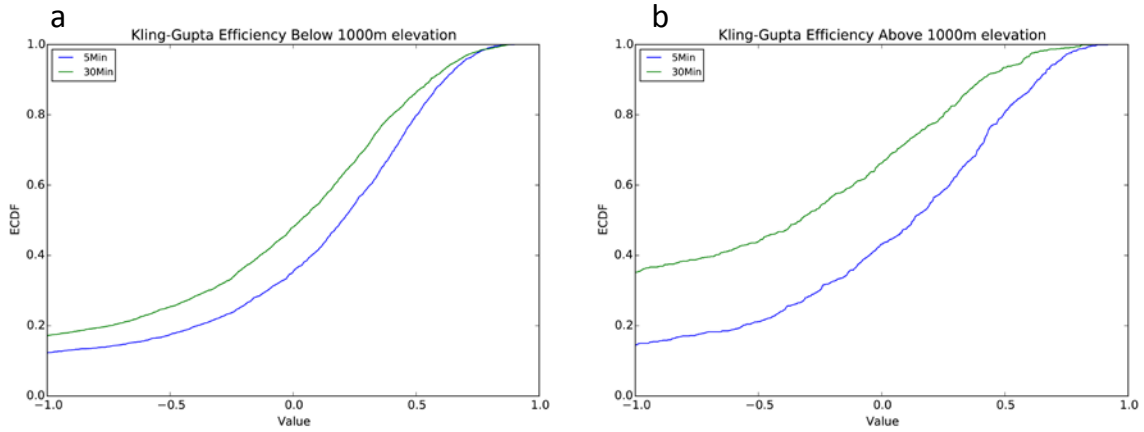

Figure 4. Cumulative frequency distributions of Kling-Gupta efficiency (KGE) values for GRDC stations that are positioned below (a) and above (b) 1000 m a.m.s.l. It can be expected that for the stations above 1000 m, the upstream area is influenced by snow dynamics.

The histograms of the anomaly correlation are shown in Figure 5. The anomaly correlations are generally lower than the correlations, showing that seasonality explains part of the skill in many regions where seasonal variation is dominant when compared to intra-annual or inter-annual variability. Clearly, the 5 arc-minute results are much better than those of the half-degree simulation, indicating a higher skill with regard to capturing inter-annual anomalies. Figure 6 shows a map of the difference between the anomaly correlation and the correlation for the 5 arc-minute case. This map shows that there are some regions where the anomaly correlation is better than the correlation (blue colours), e.g. snow-dominated regions in Canada and the Niger basin. These are catchments where the model has difficulty reproducing the correct seasonality as a result of errors in snow dynamics (Canada) or groundwater dynamics (Niger). Also, in case of the Niger River, not representing the inner delta flooding and resulting high evaporation may be the cause of poor seasonal timing of discharge.

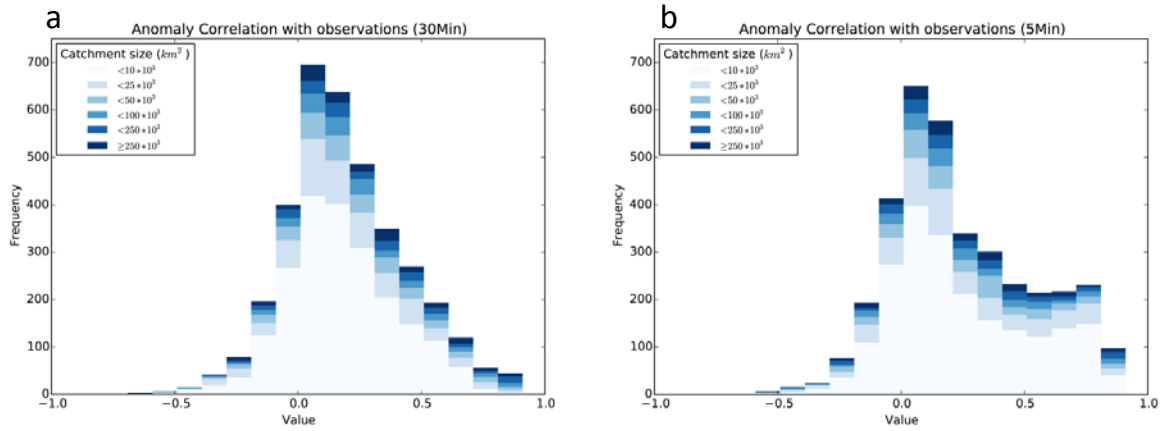

Figure 5. Histograms of evaluation statistics showing the anomaly correlation for the simulated discharge for the 30 arc-minutes and the 5 arc-minute simulations based on 3597 GRDC discharge stations, a. anomaly correlation half arc-degree simulation, b. anomaly correlation 5 arc-minute simulation.

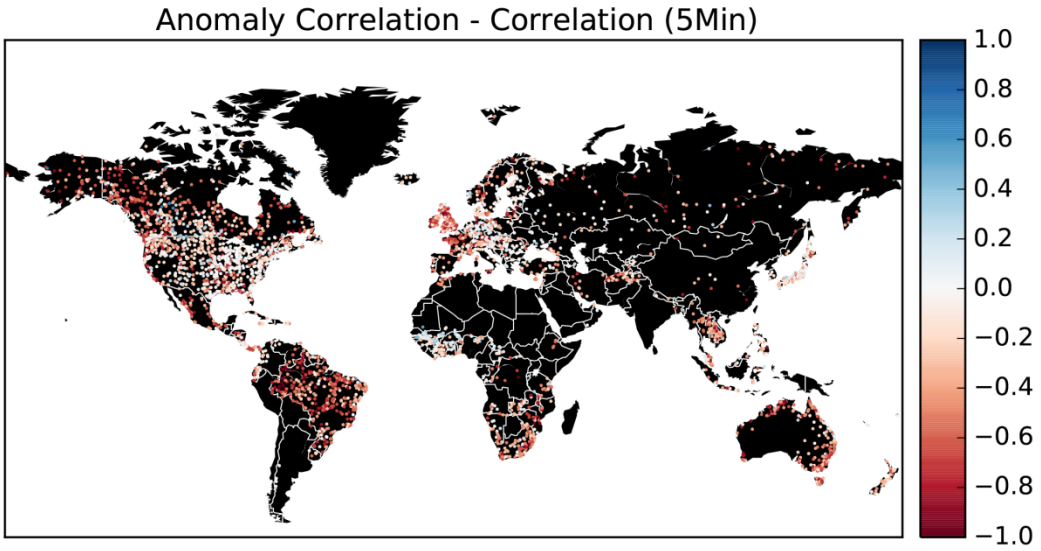

Figure 6. Map showing for the 5 arc-minute run the difference between the correlation and the anomaly correlation between simulated and observed discharge time series for 3597 GRDC discharge stations, negative values mean that the correlation is higher than the anomaly correlation.

3.4.2 Total water storage

Figure 7 compares the trends in 5 arc-minute simulated total water storage (TWS) with those from GRACE, estimated as the average change in m/year over the period 2003-2015. Generally, the PCR-GLOBWB 2 simulation is able to capture major groundwater depleted regions as suggested by GRACE, such as those in the Central Valley aquifer, the High Plains aquifer, the North China Plain aquifer, as well as parts of the Middle East, Pakistan and India. For these regions, the absolute rates of TWS change (i.e. TWS declines) of PCR-GLOBWB 2 are generally larger, while the spatial pattern in the GRACE map tends to be smoother. This is mainly due to the lower resolution and spatial averaging used in the GRACE product, as well as the fact that the current PCR-GLOBWB 2 simulation does not include lateral groundwater flow between cells. In the polar regions where GRACE estimates mass loss due to melting glaciers and ice sheets, PCR-GLOBWB 2 simulates accumulation as a result of lack of a glacier parameterization. Finally, there are some clear differences over the Amazon and some parts of Africa. A possible explanation are errors in meteorological forcing data, which is not very accurate in these parts, but also problems with the over-estimation of PCR-GLOBWB's groundwater response times in these regions which therefore fail to be sufficiently sensitive to recent changes in terrestrial precipitation.

Further analyses were conducted at the basin-scale resolution, where both TWS time series of PCR-GLOBWB 2 and GRACE *JPL-RL05M* were averaged over a river basins areas map derived from the 5 arc-minute PCR-GLOBWB drainage network. We identified all river basins with sizes larger than 900,000 km^2, which is similar to the GRACE resolution. Smaller river basins were merged to the nearest river basins or grouped together. For the remaining map of large basins, the correlations between PCR-GLOBWB 2 and GRACE basin-average monthly and annual TWS time series were calculated. Monthly correlation provides information about PCR-GLOBWB's ability to correctly time TWS seasonal variability (with a value equal to 1 for perfect timing), while the correlation for annual time series measures inter-annual variability.

The results in Figure 8 show that PCR-GLOBWB 2 is able to capture GRACE's TWS seasonality for most basins around the world, with the exception of some cold regions in high latitudes (e.g. the Yukon River basin, Iceland). This shortcoming is most likely due to the lack of a proper representation of glacier and ice processes in PCR-GLOBWB 2. As expected, the correlation values for inter-annual time series are generally lower than the ones for monthly time series. There are some areas with negative correlation values, such as the Amazon, Niger and Nile river basins. Apart from the uncertainty in the GRACE signal, these deficiencies may be related to errors in model forcing and structural errors such as errors in the groundwater response time and the effects of wetlands that have not been represented sufficiently well.

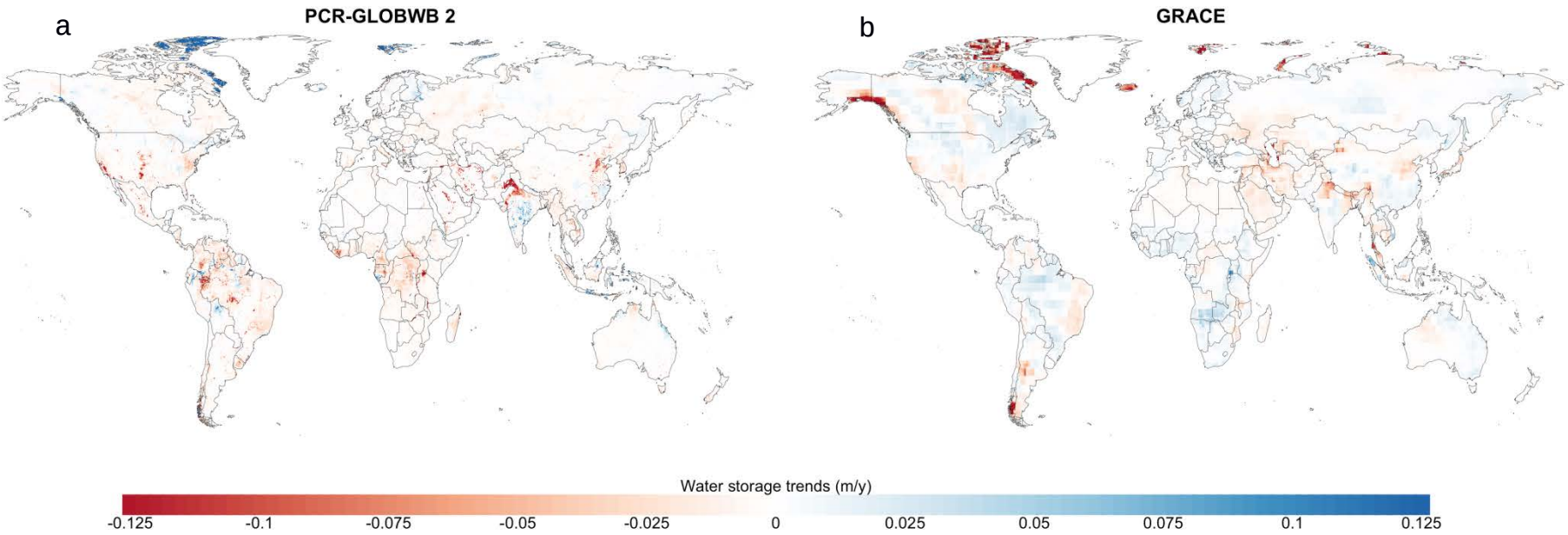

Figure 7. Comparison of PCR-GLOBWB 2 total water storage trends (m/year) with those estimated with GRACE over the period 2003-2015. a. TWS trends simulated with PCR-GLOBWB at 5 arc-minutes resolution (~10 km at the equator). Negative values indicate declining TWS (e.g. groundwater depleted regions). b. TWS trends obtained based on the GRACE JPL PL-RL05M Mascon product. The GRACE data were resampled to the resolution of 30 arc-minutes, but they actually represent the 3 x 3 arc-degree (~300 km x 300 km) area, which is the native resolution of the GRACE signal.

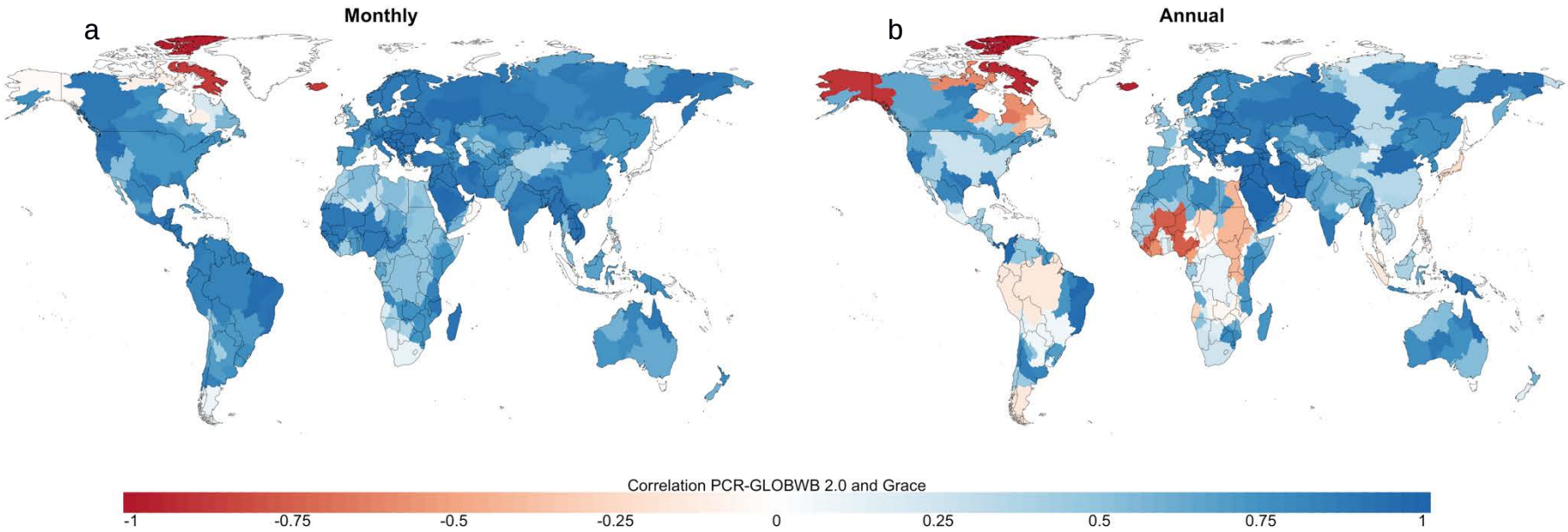

Figure 8. a. Correlation between monthly TWS time series simulated PCR-GLOBWB 2 and the GRACE JPL PL-RL05M Mascon product over the period 2003-2015. b. Comparison of annual TWS series (inter-annual variability). Comparison is only done for the larger basins over 900,000 km2, conform the 3x3 arc-degree resolution of GRACE.

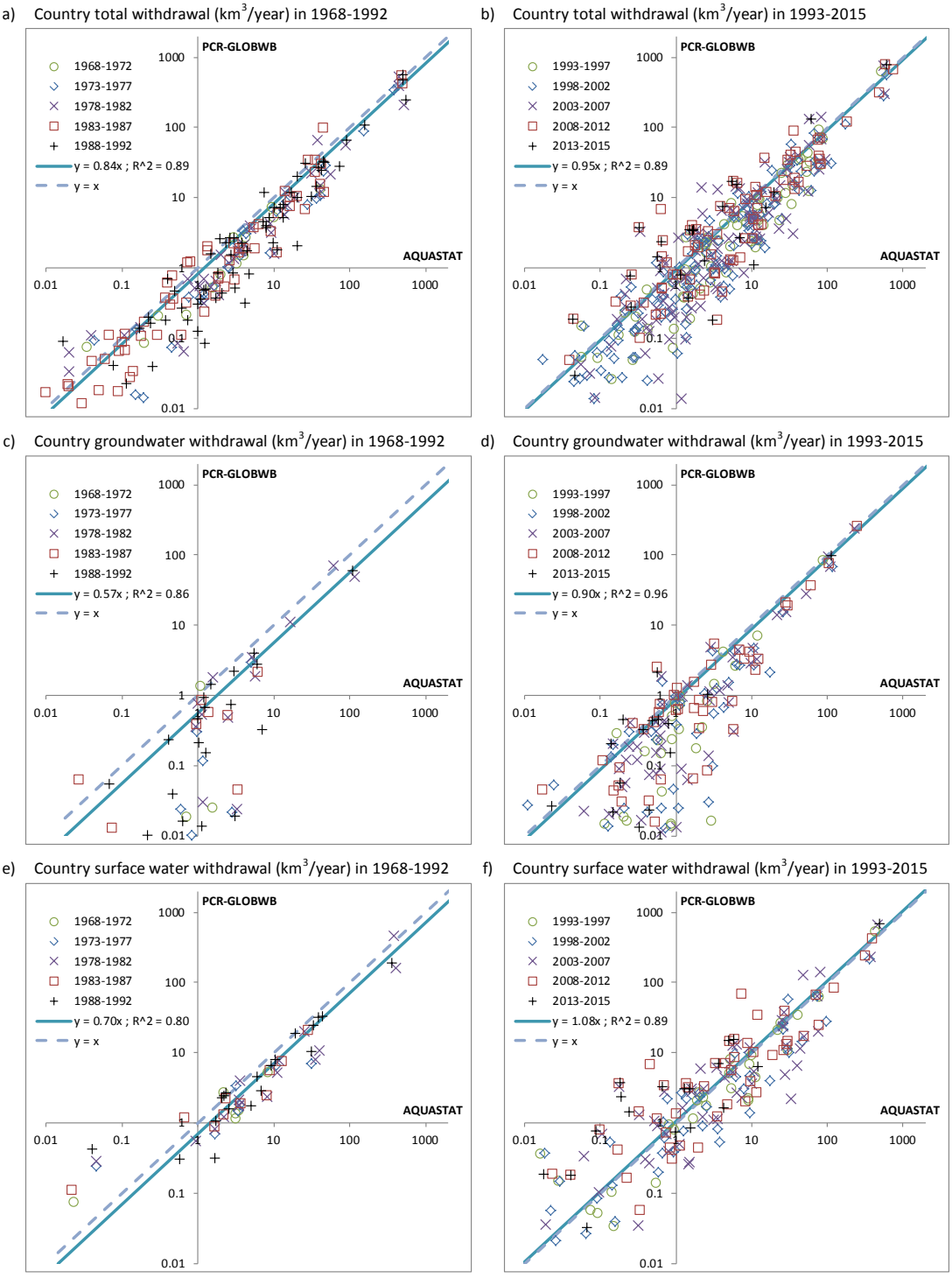

Fig. 9: Country water withdrawal (km^3/year) by source, evaluation of simulations with PCR-GLOBWB 2 with reported values in AQUASTAT (FAO, 2016). The scatterplots on the left (a, c, e) are for the period 1968-1992, while the right ones (b, d, f) are 1993-2015. The uppermost plots (a, b) are for total water withdrawal, the middle ones (c, d) are groundwater withdrawal, and the lowermost charts (e, f) are surface water withdrawal. Regression coefficient based on regression to non-log transformed data with intercept kept zero.

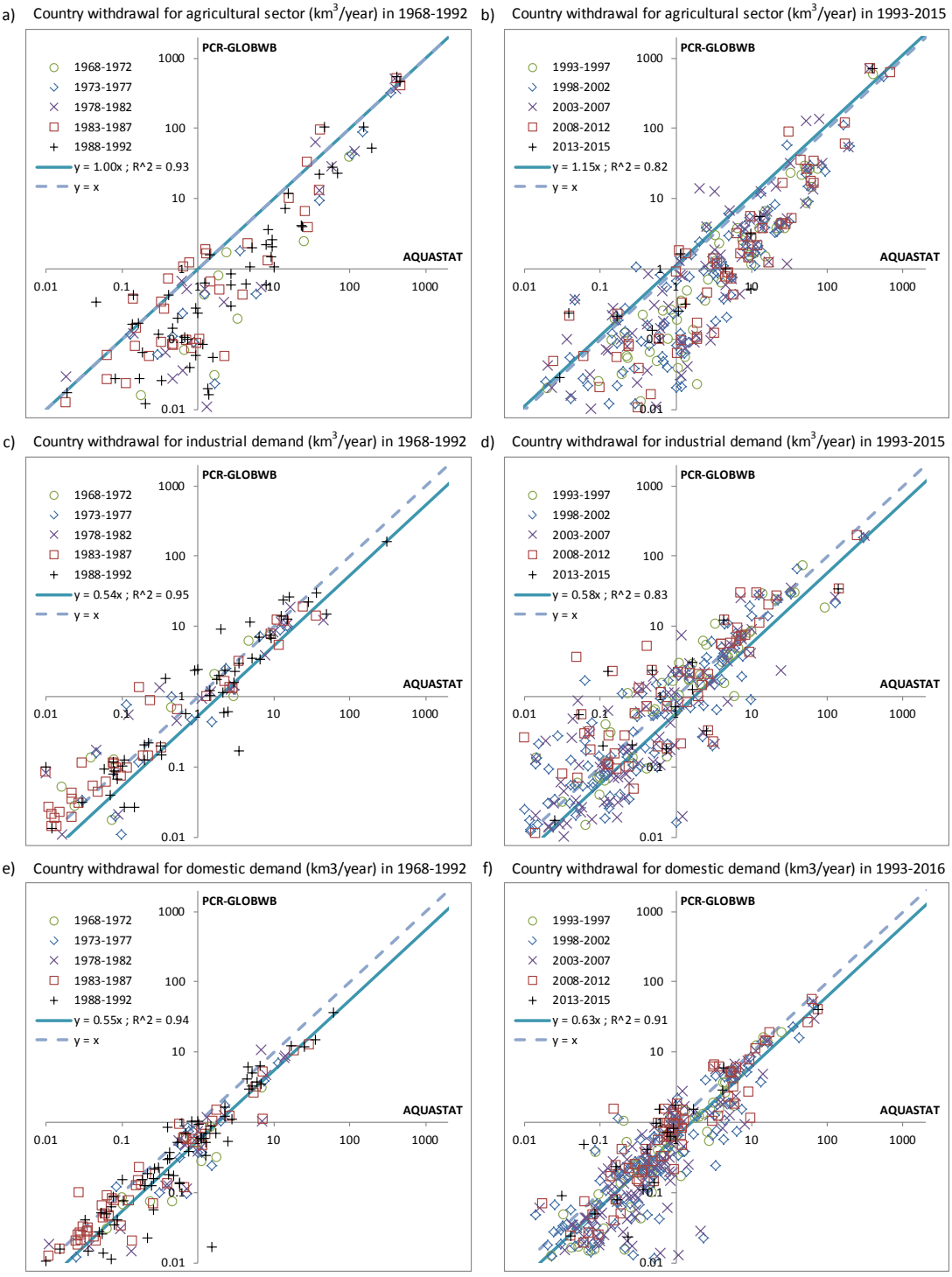

781

782 *Fig. 10: Country water withdrawal (km3/year) by sector, evaluation of simulations with PCR-GLOBWB 2*
783 *with reported values in AQUASTAT (FAO, 2016). The scatterplots on the left (a, c, e) are for the period 1968-*
784 *1992, while the right ones (b, d, f) are 1993-2015. The uppermost plots (a, b) are for withdrawal for*
785 *agricultural purpose, the middle ones (c, d) are industrial withdrawal, and the lowermost charts (e, f) are*
786 *domestic. Regression coefficient based on regression to non-log transformed data with intercept kept zero.*

787

3.4.3 Water withdrawal

We compared simulated water withdrawal data from PCR-GLOBWB 2 with reported withdrawal data per country from AQUASTAT (FAO, 2016). The results are shown subdivided per source (Figure 9) and per sector (Figure 10).. Total water withdrawal and surface water withdrawal are simulated reasonably well (R^2 between 0.84 and 0.96 and regression slopes between 0.70 and 1.08). However, groundwater withdrawal is underestimated for the smaller water users. A likely explanation for this is occasional groundwater withdrawal by farmers during dry periods in areas that have not been mapped as irrigated crops in MIRCA, such as grasslands in e.g. Germany and the Netherlands, while this groundwater withdrawal is reported in AQUASTAT.

When looking at water withdrawal per sector, results are mixed. The largest agricultural water users are well captured, but the smaller ones are clearly underestimated. This is related to the fact that in many regions of the smaller water use countries, water is used for irrigation only occasionally during dry summers, while these areas are not mapped as irrigated crops in MIRCA. Also, many of these countries use irrigation technology that is not part of MIRCA, e.g. subsurface drainage by artificially high surface water levels such as in a number developed delta regions in the world. However, even though these smaller countries are not well represented, PCR-GLOBWB 2 is still able to capture the big water users, which have a significant impact on the water cycle and are most important for global scale analyses.

Both industrial and domestic water withdrawals are underestimated. The underestimation of industrial water withdrawal is partly caused by the fact that we do not include water withdrawal for thermo-electric cooling of power plants. The underestimation of domestic water withdrawal comes from the fact that we assume that the priority of water allocation is proportional to demand. This means that in times of shortage, water withdrawal is reduced with an equal percentage for agriculture, industry and domestic use. In many countries however, there is a priority series, whereby domestic demand is first met, industrial demand next and agricultural demand comes last. As a result, we underestimate domestic water withdrawal and it also partly causes the underestimation of industrial water withdrawal. This is corroborated by plotting gross water demand (which would be withdrawal if no shortage would occur) against AQUASTAT data. These plots (not shown here) result in a regression slopes of 0.68-0.75 for industrial demand and 0.78-0.92 for domestic demand. These results thus reveal that the water allocation scheme of PCR-GLOBWB 2 should be further improved.

4. Conclusions and future work

We presented the most recent version of the open source global hydrology and water resources model PCR-GLOBWB. This version, PCR-GLOBWB 2, has a global coverage at 5 arc-minute resolution. Apart from the higher resolution, the new model has an integrated water use scheme, i.e. every day sector specific water demand is calculated, resulting in groundwater and surface water withdrawal, water consumption and return flows. Dams and reservoirs from the GranD database (Lehner et al., 2011) are added progressively according to their year of construction. PCR-GLOBWB 2 has been rewritten in Python and uses PCRaster-Python functions (Karssenberg et al., 2007). It has a modular structure, which makes the replacement and maintenance of model parts easier. PCR-GLOBWB 2 can be dynamically coupled to a global 2-layer groundwater model (de Graaf et al., 2017; Sutanudjaja et al., 2014; Sutanudjaja et al., 2011) and a one-way coupling to hydrodynamic models for large-scale inundation modelling (Hoch et al., 2017b) is also available.

Comparing the 5 arc-minute with 30 arc-minute simulations using discharge data we clearly find an improvement in the model performance of the higher resolution model. We find a general increase in correlation, anomaly correlation and KGE, indicating that the higher resolution model is better able to capture the seasonality, inter-annual anomalies and the general discharge characteristics. Also, PCR-GLOBWB 2 is able to reproduce trends and seasonality in total water storage as observed by GRACE for most river basins. It simulates the hotspots of groundwater decline that around in GRACE as well. Simulated total water withdrawal matches reasonably well with reported water withdrawal from AQUASTAT, while water withdrawal by source and sector provide mixed results.

Future work will concentrate on further improving the water withdrawal and water allocation scheme, developing a full dynamic (two-way) coupling with hydrodynamic models, developing 5 km and 1 km resolution (or higher) parameterizations of PCR-GLOBWB 2 using scale-consistent parameterizations (e.g. using MPR, Samaniego et al., 2017), incorporating a crop growth model and solving the full surface energy balance. Other foreseeable developments are using the model in probabilistic settings and in data-assimilation frameworks.

5. Code and data availability

PCR-GLOBWB 2 is open source and distributed under the terms of the GNU General Public License version 3, or any later version, as published by the Free Software Foundation. The model code is provided through a Github repository: https://github.com/UU-Hydro/PCR-GLOBWB_model (Sutanudjaja et al., 2017a, https://doi.org/10.5281/zenodo.595656). This keeps users and developers immediately aware of any new revisions. Also, it allows developers to easily collaborate, as they can download a new version, make changes, and suggest and upload the newest revisions. The configuration ini-files for the global 30 arc-minutes and 5arc-minute models and the associated model parameters and input files are provided on https://doi.org/10.5281/zenodo.1045338 (Sutanudjaja et al., 2017b). Development and maintenance of the official version (main branch) of PCR-GLOBWB 2 is conducted at the Department of Physical Geography, Utrecht University. Yet, contributions from external parties are welcome and encouraged. For news on latest developments and papers published based on PCR-GLOBWB 2 we refer to http://www.globalhydrology.nl and for the underlying PCRaster-Python code to http://pcraster.geo.uu.nl.

Acknowledgements

We thank Utrecht University and various grants and projects that directly or indirectly contributed to the development of PCR-GLOBWB 2. The authors are very grateful to all the contributors (as acknowledged in the references) who provided the data sets used in this study. We acknowledge the Netherlands Organisation for Scientific Research (NWO) for the grant that enabled us to use the national super computer Cartesius with the help of SURFsara Amsterdam. The authors thank two anonymous reviewers for their constructive comments and suggestions that helped to improve the manuscript. We are also grateful to the Editors for their efficient handling of the review process.

Appendix

Table A1 - List (non-exhaustive) of state and flux variables defined in PCR-GLOBWB

Description	Symbol	Unit
Interception storage	S_{int}	m
Snow cover/storage in water equivalent thickness (excluding liquid part S_{slq})	S_{swe}	m
Liquid/melt water storage in the snow pack	S_{slq}	m
Upper and lower soil storages	S_1 and S_2	m
Surface water storage (lakes, reservoirs, rivers and inundated water)	S_{wat}	m
groundwater storage (renewable part)	S_3	m
fossil groundwater storage (non-renewable)	S_{nrw}	m
total groundwater storage = $S_3 + S_{nrw}$	S_{gwt}	m
total water storage thickness = $S_{int} + S_{swe} + S_{slq} + S_1 + S_2 + S_{gwt}$	TWS	m
potential evaporation	E_{pot}	$m.day^{-1}$
evaporation flux from the intercepted precipitation	E_{int}	$m.day^{-1}$
evaporation from melt water stored in the snow pack	E_{slq}	$m.day^{-1}$
bare soil evaporation	E_{soil}	$m.day^{-1}$
transpiration from the upper and lower soil stores	T_1 and T_2	$m.day^{-1}$
total land evaporation = $E_{pot} + E_{int} + E_{slq} + E_{soil} + T_1 + T_2$	E_{land}	$m.day^{-1}$
surface water evaporation	E_{wat}	$m.day^{-1}$
total evaporation = $E_{land} + E_{wat}$	E_{tot}	$m.day^{-1}$
direct runoff	Q_{dr}	$m.day^{-1}$
interflow, shallow sub-surface flow	Q_{sf}	$m.day^{-1}$
baseflow, groundwater discharge	Q_{bf}	$m.day^{-1}$
specific runoff from land	Q_{loc}	$m.day^{-1}$
local change in surface water storage	Q_{wat}	$m.day^{-1}$
total specific runoff	Q_{tot}	$m.day^{-1}$
routed channel (surface water) discharge	Q_{chn}	$m^3.sec^{-1}$
net fluxes from the upper to lower soil stores	Q_{12}	$m.day^{-1}$
net groundwater recharge, fluxes from the lower soil to groundwater stores	RCH = Q_{23}	$m.day^{-1}$
surface water infiltration to groundwater	Inf	$m.day^{-1}$
desalinated water withdrawal	W_{sal}	$m.day^{-1}$
surface water withdrawal	W_{wat}	$m.day^{-1}$
renewable groundwater withdrawal	W_3	$m.day^{-1}$
non-renewable groundater withdrawal (groundwater depletion)	W_{nrw}	$m.day^{-1}$
total groundwater withdrawal = $W_3 + W_{nrw}$	W_{gwt}	$m.day^{-1}$
water withdrawal allocated for irrigation purpose	A_{irr}	$m.day^{-1}$
water withdrawal allocated for livestock demand/sector	A_{liv}	$m.day^{-1}$
water withdrawal allocated for agricultural sector = $A_{irr} + A_{liv}$	A_{agr}	$m.day^{-1}$
domestic water withdrawal	A_{dom}	$m.day^{-1}$
industrial water withdrawal	A_{ind}	$m.day^{-1}$

Table A2 - List of model inputs and parameters

Description	Symbol	Unit	References/sources
Upper and lower soil store parameters:			FAO (2007) soil map; van Beek and Bierkens (2009)
- Soil thickness	Z_1 and Z_2	m	
- Residual soil moisture content	θ_{r-1} and θ_{r-2}	$m^3.m^{-3}$	
- Soil moisture at saturation	θ_{s-1} and θ_{s-2}	$m^3.m^{-3}$	
- Soil water storage capacity per soil layer: $SC = Z / (\theta_s - \theta_r)$	SC_1 and SC_2	m	
- Soil matric suctions at saturation	ψ_{s-1} and ψ_{s-2}	m	
- Exponent in the soil water retention curve	β_1 and β_2	dimensionless	
- Saturated hydraulic conductivities of upper and lower soil stores	K_1 and K_2	$m.day^{-1}$	
- Total soil water storage capacities = $SC_{upp} + SC_{low}$	W_{max}	m	
Land cover fraction: Land cover areas (including extent of irrigated areas) over cell areas	f_{lcov}	$m^2.m^{-2}$	GLCC v2.0 map (USGS, 1997); Olson (1994a, 1994b); MIRCA2000 dataset (Portmann et al., 2010), FAOSTAT (2012)
Topographical parameters	DEM	m	HydroSHEDS (Lehner et al., 2008); Hydro1k (Verdin and Greenlee, 1996); GTOPO30 (Gesch et al., 1999)
- Cell-average DEM	DEM_{avg}	m	
- Flood plain elevation	DEM_{fpl}	m	
Root fractions per soil layer	Rf_{upp} & Rf_{low}	dimensionless	Canadell et al. (1996); van Beek and Bierkens (2009)
Arno scheme (Todini, 1999; Hagemann and Gates, 2003) exponents defining soil water capacity distribution	β_{arno}	dimensionless	Canadell et al. (1996), Hagemann et al. (1999); Hagemann (2002); van Beek (2008); van Beek and Bierkens (2009)
Ratios of cell-minimum and cell-maximum soil storage to W_{max}	f_{wmin} and f_{wmax}	m	van Beek (2008); van Beek and Bierkens (2009)

884

885
886

887

888

Table A2 - List of model inputs and parameters (continued)

Description	Symbol	Unit	References/sources
Parameters related to phenology			Hagemann et al. (1999); Hagemann (2002); van Beek (2008); van Beek and Bierkens (2009)
- Crop coefficient	K_c	dimensionless	
- Interception capacity	$S_{int\text{-}max}$	m	
- Vegetation cover fraction	C_v	$m^2.m^{-2}$	
Groundwater parameters			GLHYMPS map (Gleeson et al., 2014); van Beek (2008); van Beek and Bierkens (2009)
- Aquifer transmissivity	*KD*	$m^2.day^{-1}$	
- Aquifer specific yield	*Sy*	$m^3.m^{-3}$	
- Groundwater recession coefficient	*J*	day^{-1}	
Meteorological forcing			van Beek (2008); CRU (Harris et al., 2014); ERA40 (Uppala et al., 2005); ERA-Interim (Dee et al., 2011)
- Total precipitation	*P*	$m.day^{-1}$	
- Atmospheric air temperature	T_{air}	°C or K	
- Reference potential evaporation and transpiration	$E_{ref,pot}$	$m.day^{-1}$	
Others:			
- Non-irrigation sectoral water demand (i.e. livestock, dometic and industrial)		$m.day^{-1}$	Wada et al (2014)
- Desalinated water		$m.day^{-1}$	Wada et al., (2011a); FAO (2016)
- Lakes and reservoirs			GLWD1 (Lehner and Döll, 2004); GranD (Lehner et al., 2011)

References

Alfieri, L., Burek, P. Dutra, E. Krzeminski, B. Muraro, D. Thielen, J., and Pappenberger F.: GloFAS—Global ensemble streamflow forecasting and flood early warning, Hydrology and Earth System Science, 17, 1161–1175, 2003.
Allen, R.G., Pereira, L.S., Raes, D., and Smith, M.: Crop evaporation: Guidelines for computing crop requirements., UN-FAO, Rome, Italy, 1998.
Argent, R. M.: An overview of model integration for environmental applications–components, frameworks and semantics, Environmental Modelling & Software 19 (3): 219–34, doi:10.1016/S1364-8152(03)00150-6, 2004.
Bates, P.D., Horritt, M. S., and Fewtrell, T.J.: A simple inertial formulation of the shallow water equations for efficient twodimensional flood inundation modelling, Journal of Hydrology, 38, 33–45, 2010.
Bergström, S.: The HBV model, in: Computer Models in Watershed Hydrology, edited by Singh, V. P., Water Resources Publications, Highlands Ranch, CO, 1995.
Beven, K.J. and Cloke, H.L.: Comment on "Hyperresolution global land surface modeling: Meeting a grand challenge for monitoring Earth's terrestrial water" by Eric F. Wood et al., Water Resources Research, 48, 2012.
Bierkens, M.F.P. and van Beek, L.P.H.: Seasonal Predictability of European Discharge: NAO and Hydrological Response Time, Journal of Hydrometeorology 10, 953–968, 2009.
Bierkens, M.F.P., Bell, V.A., Burek, P., Chaney, N., Condon, L.E., David, C.H., de Roo, A., Döll, P., Drost, N., Famiglietti, J. S., Flörke, M., Gochis, D. J., Houser, P., Hut, R., Keune, J., Kollet, S., Maxwell, R. M., Reager, J. T., Samaniego, L., Sudicky, E., Sutanudjaja, E. H., van de Giesen, N., Winsemius, H., and Wood, E. F.: Hyper-resolution global hydrological modelling: what is next? "Everywhere and locally relevant", Hydrological Processes, 29, 310-320, 2014.
Bos, M.G.: Discharge measurement structures, third revised edition, ILRI Wageningen, 1989.
Bosmans, J. H. C., van Beek, L. P. H., Sutanudjaja, E. H., and Bierkens, M. F. P.: Hydrological impacts of global land cover change and human water use, Hydrol. Earth Syst. Sci., 21, 5603-5626, https://doi.org/10.5194/hess-21-5603-2017, 2017.
Campbell, G. S.: A simple method for determining unsaturated conductivity from moisture retention data, Soil Science, 117, 311–314, 1974.
Canadell, J., Jackson, R.B., Ehleringer, J.B. et al: Maximum rooting depth of vegetation types at the global scale, Oecologia, https://doi.org/10.1007/BF00329030, 1996.
Candogan Yossef, N., Winsemius, H. Weerts, A. van Beek, L. P. H, and Bierkens, M.F.P.: Skill of a global seasonal streamflow forecasting system, relative roles of initial conditions and meteorological forcing, Water Resources Research 49, 4687–4699, 2013.
Castronova, A. M. and Goodal, J. L.: A generic approach for developing process-level hydrologic modeling components." Environmental Modelling & Software 25 (7): 819–25. doi:10.1016/j.envsoft.2010.01.003, 2010.
Clapp, R. B. and Hornberger, G. M.: Empirical equations for some soil hydraulic properties, Water Resources Research, 14, 601–604, 1978.
Cohen, S., Kettner, A. J., Syvitski, J. P. M., and Fekete, B. A. M.: WBMsed, a distributed global-scale riverine sediment flux model: Model description and validation, Computers in Geosciences, 53, 80–93, 2013.
Dalin, C., Wada, Y., Kastner, T., and M. J. Puma: Groundwater depletion embedded in international food trade, Nature, 543, 700–704, 2017.
Dankers, R., Arnell, N. W., Clark, D. B., Falloon, P. D., Fekete, B. M., Gosling, S. N., Heinke, J., Kim, H., Masaki, Y., Satoh, Y., Stacke, T., Wada, Y., and Wisser, D.: First look at changes in flood hazard in the Inter-Sectoral Impact Model Intercomparison Project ensemble, Proceedings of the National Academy of Sciences, 2013.
De Graaf, I. E. M., van Beek, L. P. H., Wada, Y., and Bierkens, M. F. P.: Dynamic attribution of global water demand to surface water and groundwater resources: Effects of abstractions and return flows on river discharges, Advances in Water Resources 64, 21–33, 2014.
De Graaf, I. E. M., Sutanudjaja, E. H., Van Beek, L. P. H., and Bierkens, M. F. P.: A high-resolution global-scale groundwater model. Hydrology and Earth System Sciences, 19, 823-837, 2015.
De Graaf, I. E., van Beek, L.P.H., Gleeson, T., Moosdorf, N., Schmitz, O., Sutanudjaja, E. H., and Bierkens, M. F. P.: A global-scale two-layer transient groundwater model: Development and application to groundwater depletion. Advances in Water Resources, 102, 53-67, 2017.
Dee, D. P., Uppala, S. M., Simmons, A. J., Berrisford, P., Poli, P., Kobayashi, S., Andrae, U., Balmaseda, M. a., Balsamo, G., Bauer, P., Bechtold, P., Beljaars, a. C. M., van de Berg, L., Bidlot, J., Bormann, N., Delsol, C., Dragani, R., Fuentes, M., Geer, a. J., Haimberger, L., Healy, S. B., Hersbach, H., Hólm, E. V., Isaksen, L., Kå llberg, P., Köhler, M., Matricardi, M., McNally, a. P.,

949 Monge-Sanz, B. M., Morcrette, J.-J., Park, B.-K., Peubey, C., de Rosnay, P., Tavolato, C., Thépaut,
950 J.-N., and Vitart, F.: The ERA-Interim reanalysis: configuration and performance of the data
951 assimilation system, Quarterly Journal of the Royal Meteorological Society, 137, 553–597, 2011.
952 Dermody, B. J., van Beek, L. P. H., Meeks, E., Klein Goldewijk, K., Scheidel, W., van der Velde, Y.,
953 Bierkens, M. F. P., Wassen, M. J., and Dekker, S. C.: A virtual water network of the Roman world,
954 Hydrology and Earth System Sciences, 18, 5025–5040, http://dx.doi.org/10.5194/hess-18-5025-
955 2014, 2014.
956 Döll, P. and Siebert, S.: Global modeling of irrigation water requirements, Water Resources Research,
957 38, 8–1 – 8–10, 2002.
958 Döll, P., Kaspar, F., and Lehner, B.: A global hydrological model for deriving water availability
959 indicators: model tuning and validation, Journal of Hydrology, 270, 105–134, 2003.
960 Döll, P., Hoffmann-Dobrev, H., Portmann, F. T., Siebert, S., Eicker, A., Rodell, M., Strassberg, G., and
961 Scanlon, B. R.: Impact of water withdrawals from groundwater and surface water on continental
962 water storage variations, Journal of Geodynamics, 59–60, 143–156, 2012.
963 Döll, P., Muller Schmied, H., Schuh, Portmann, F. T. and Eicker, A.: Global-scale assessment of
964 groundwater depletion and related groundwater abstractions: Combining hydrological modeling
965 with information from well observations and GRACE satellites, Water Resources Research, 50,
966 2014.
967 Doorenbos, J. and Pruitt, W. O.: Crop water requirements, Irrig. Drain. Pap. 24, FAO, Rome, 1977.
968 Elliott, J., Deryng, D., Müller, C., Frieler, K., Konzmann, M., Gerten, D., Glotter, M., Flörke, M.,
969 Wada, Y., Best, N., Eisner, S., Fekete, B. M., Folberth, C., Foster, I., Gosling, S. N., Haddeland, I.,
970 Khabarov, N., Ludwig, F., Masaki, Y., Olin, S., Rosenzweig, C., Ruane, A. C., Satoh, Y., Schmid,
971 E., Stacke, T., Tang, Q., and Wisser, D.: Constraints and potentials of future irrigation water
972 availability on agricultural production under climate change, Proceedings of the National Academy
973 of Sciences, 111, 3239–3244, 2013.
974 Erkens, G. and Sutanudjaja, E. H.: Towards a global land subsidence map, Proc. IAHS, 372, 83-87,
975 https://doi.org/10.5194/piahs-372-83-2015, 2015.
976 Fekete, B. M. B., Vörösmarty, C. J. C., and Grabs, W.: High-resolution fields of global runoff
977 combining observed river discharge and simulated water balances, Global Biogeochemical Cycles,
978 16, 10–15, 2002.
979 Food and Agriculture Organization of the United Nations (FAO): Digital Soil Map of the World,
980 Version 3.6. FAO, Rome, Italy, 2007.
981 Food and Agriculture Organization of the United Nations (FAO): FAOSTAT statistics database,
982 http://www.fao.org/faostat/en/#home, 2012.
983 Food and Agriculture Organization of the United Nations (FAO): AQUASTAT database of water-
984 related data. Accessed on [2017-09-15] at: http://www.fao.org/nr/water/aquastat/main/index.stm,
985 2016.
986 Gesch, D.B., Verdin, K.L., and Greenlee, S.K.: New Land Surface Digital Elevation Model Covers the
987 Earth: Eos, Transactions, American Geophysical Union, v. 80, no. 6, p. 69–70, 1999.
988 Gleeson, T., Wada, Y., Bierkens, M. F. P., and van Beek, L. P. H.: Water balance of global aquifers
989 revealed by groundwater footprint, Nature, 488, 197–200, 2012.
990 Gleeson, T., N. Moosdorf, J. Hartmann, and L. P. H. van Beek: A glimpse beneath earth's surface:
991 GLobal HYdrogeology MaPS (GLHYMPS) of permeability and porosity, Geophys. Res. Lett., 41,
992 3891–3898, doi:10.1002/2014GL059856, 2014.
993 Global Soil Data Task: Global Soil Data Products CD-ROM (IGBP-DIS), 2000.
994 Gosling, S. N. and Arnell, N.W.: Simulating current global river runoff with a global hydrological
995 model: model revisions, validation, and sensitivity analysis, Hydrological Processes, 25, 1129–
996 1145, 2011.
997 Gupta, H.V., Kling, H., Yilmaz, K.K., and Martinez, G.F.: Decomposition of the mean squared error
998 and NSE performance criteria: Implications for improving hydrological modelling. Journal of
999 Hydrology,377, 80-91, 2009.
1000 Haddeland, I., Heinke, J., Biemans, H., Eisner, S., Flörke, M., Hanasaki, N., Konzmann, M., Ludwig,
1001 F., Masaki, Y., Schewe, J., Stacke, T., Tessler, Z. D., Wada, Y., and Wisser, D.: Global water
1002 resources affected by human interventions and climate change, Proceedings of the National
1003 Academy of Sciences, 111, 3251–3256, 2014.
1004 Hagemann, S., Botzet, M., Dümenil, L., and Machenhauer, B.: Derivation of Global GCM Boundary
1005 Conditions from 1 Km Land Use Satellite Data, Max-Planck-Institut für Meteorologie, Hamburg,
1006 Germany, 1999.

Hagemann, S.: An improved land surface parameter dataset for global and regional climate models, Max- Planck-Institut für Meteorologie, Hamburg, Germany, https://www.mpimet.mpg.de/fileadmin/publikationen/Reports/max_scirep_336.pdf, 2002.
Hagemann, S. and Gates, L.D.: Improving a subgrid runoff parameterization scheme for climate models by the use of high resolution data derived from satellite observations, Climate Dynamics, 21, 349–359, 2003.
Hagemann, S., Botzet, M., Dümenil, L., and Machenhauer, B.: Derivation of Global GCM Boundary Conditions from 1 Km Land Use Satellite Data, Max-Planck-Institut für Meteorologie, Hamburg, Germany, 1999.
Hamon, W.: Computation of Direct Runoff Amounts from Storm Rainfall, IAHS Publ., 63, 52–62, 1963.
Hanasaki, N., Kanae, S., Oki, T., Masuda, K., Motoya, K., Shirakawa, N., Shen, Y., and Tanaka, K.: An integrated model for the assessment of global water resources - Part 1: Model description and input meteorological forcing, Hydrology and Earth System Science, 12, 1007–1025, 2008.
Hanasaki, N., S. Kanae, T. Oki, K. Masuda, K. Motoya, N. Shirakawa, Y. Shen, and K. Tanaka (2008b), An integrated model for the assessment of global water resources - Part 2: Applications and assessments, Hydrology and Earth System Science, 12, 1027–103.
Hanasaki, N., Yoshikawa, S., Pokhrel, Y.and Kanae, S. A global hydrological simulation to specify the sources of water used by humans Hydrology and Earth System Science, 22, 789-817, 2018
Harbaugh, A.W., Banta, E.R., Hill, M.C., and McDonald, M.G., 2000, MODFLOW-2000, the U.S. Geological Survey modular ground-water model -- User guide to modularization concepts and the Ground-Water Flow Process: U.S. Geological Survey Open-File Report 00-92, 121 p
Harris, I., Jones, P., Osborn, T., and Lister, D.: Updated high-resolution grids of monthly climatic observations - the CRU TS3.10 Dataset, International Journal of Climatology, 34, 623–642, 2014.
Hirabayashi Y., M. Roobavannan, K. Sujan, K. Lisako, Y. Dai, W. Satoshi, K. Hyungjun, and K. Shinjiro (2013), Global flood risk under climate change, Nature Climate Change, 3, 816–821.
Hoch, J.M., Haag, Arjen, van Dam, Arthur, Winsemius, Hessel, van Beek, L.P.H. & Bierkens, M.F.P.: Assessing the impact of hydrodynamics on large-scale flood wave propagation - a case study for the Amazon Basin, Hydrology and Earth System Science, 21, 117-132, 2017a.
Hoch, J.M., Neal, J.C., Baart, F. van Beek, L.P.H., Winsemius, H.C., Bates, P.D., and Bierkens, M.F.P.: GLOFRIM v1.0 – A globally applicable computational framework for integrated hydrological-hydrodynamic modelling. Geoscientific Model Development, 10, 3913-3929, 2017b.
Karssenberg, D., de Jong K., and van der Kwast, J.: Modelling landscape dynamics with Python, International Journal of Geographical Information Science, 21, 483-495, 2007.
Karssenberg, D., Schmitz, O., Salamon, P., de Jong, K., and Bierkens, M. F. P.: A software framework for construction of process-based stochastic spatio-temporal models and data assimilation, Environmental Modelling & Software, 25, 489–502, 2010.
Kauffeldt, A., Wetterhall, F., Pappenberger, F., Salamon, P., and Thielen, J.: Technical review of large-scale hydrological models for implementation in operational flood forecasting schemes on continental level. Environmental Modelling and Software, 75, 68–76, 2016.
Kernkamp, H.W.J., van Dam, A., Stelling, G.S. and de Goede, E.D.: Efficient scheme for the shallow water equations on unstructured grids with application to the Continental Shelf, Ocean Dynamics. 61, 1175–1188, 2011.
Konar, M., Hussein, Z., Hanasaki, N., Mauzerall, D. L., and Rodriguez-Iturbe, I.: Virtual water trade flows and savings under climate change, Hydrology and Earth System Science, 17, 3219–3234, 2013.
Konikow, L. F.: Contribution of global groundwater depletion since 1900 to sea-level rise, Geophysical Research Letters 38, L17401, 1-5, 2011.
Kraijenhoff van de Leur, D.A.: A study of non-steady ground-water flow with special reference to the reservoir-coefficient, De Ingenieur 19, 87-94, 1958.
Lehner, B. and Döll, P.: Development and validation of a global database of lakes, reservoirs and wetlands, Journal of Hydrology 296, 1–22, 2004.
Lehner, B., Verdin, K., and Jarvis, A.: New global hydrography derived from spaceborne elevation data, Eos (Washington. DC)., 89, DOI: 10.1029/2008EO100001, 2008.
Lehner, B., Reidy Liermann, C., Revenga, C., Vörösmarty, C., Fekete, B., Crouzet, P., Döll, P., Endejan, M., Frenken, K., Magome, J., Nilsson, C., Robertson, J., Rödel, R., Sindorf, N., and Wisser, D.: High- resolution mapping of the world's reservoirs and dams for sustainable river-flow management. Frontiers in Ecology and the Environment, 9 494–502, 2011.

Liang, X., Lettenmaier, D. P., Wood, E. F., and Burges, S. J.: A simple hydrologically based model of land surface water and energy fluxes for general circulation models, Journal of Geophysical Research, 99, 14415–14428, 1994.
Loveland, T. R., Reed, B. C., and Brown, J. F.: Development of a global land cover characteristics database and IGBP DISCover from 1 km AVHRR data, International Journal of Remote Sensing, 21, 1303–1330, 2000.
McDonald, R. I., Weber, K., Padowski, J., Flörke, M., Schneider, C., Green, P. A., Gleeson, T. Eckman, S. Lehner, B. Balk, D., Boucher, T. Grill, G. and Montgomery, M.: Water on an urban planet: Urbanization and the reach of urban water infrastructure. Global Environmental Change, 27, 96-105, 2011.
Murray, F.: On the computation of saturation vapor pressure, IAHS Publ., 6, 203–204, 1967.
New, M., Lister, D., Hulme, M., and Makin, I.: A high-resolution data set of surface climate over global land areas, Climate Research, 21, 1–25, 2002.
Nijssen, B., O'Donnell, G. M., Lettenmaier, D. P., Lohmann, D., and Wood, E. F.: Predicting the Discharge of Global Rivers, Journal of Climate, 14, 3307–3323, 2001.
Oki, T. and Kanae, S.: Global hydrological cycles and world water resources, Science, 313, 1068–1072, 2006.
Olson, J. S.: Global ecosystem framework-definitions, Tech. rep., USGS EROS Data Center Internal Report, Sioux Falls, SD, 1994a.
Olson, J. S.: Global ecosystem framework-translation strategy, Tech. rep., USGS EROS Data Center Internal Report, Sioux Falls, SD, 1994b.
Pappenberger, F., Dutra, E., Wetterhall, F., and Cloke, H.L.: Deriving global flood hazard maps of fluvial floods through a physical model cascade, Hydrology and Earth System Science, 16, 4143–4156, 2012.
Pokhrel, Y. N., Hanasaki, N., Yeh, P. J., Yamada, T. J., Kanae, S., and Oki, T.: Model estimates of sea-level change due to anthropogenic impacts on terrestrial water storage. Nature Geoscience, 5, 389-392, 2012.
Pokhrel, Y. N., Koirala, S. Yeh, P. J.-F., Hanasaki, N., Longuevergne, L., Kanae, S., and Oki, T.: Incorporation of groundwater pumping in a global Land Surface Model with the representation of human impacts, Water Resources Research, 51, 2015.
Portmann, F. T., Siebert, S., and Döll, P.: MIRCA2000-Global monthly irrigated and rainfed crop areas around the year 2000: A new high-resolution data set for agricultural and hydrological modeling, Global Biogeochemical Cycles, GB1011, 1-24, 2010.
Prudhomme, C., Giuntoli, I., Robinson, E. L., Clark, D. B., Arnell, N. W., Dankers, R., Fekete, B. M., Franssen, W., Gerten, D., Gosling, S. N., Hagemann, S., Hannah, D. M., Kim, H., Masaki, Y., Satoh, Y., Stacke, T., Wada, Y., and Wisser, D.: Hydrological droughts in the 21st century, hotspots and uncertainties from a global multimodel ensemble experiment, Proceedings of the National Academy of Sciences, 111, 3262–3267, 2013.
Rodell, M., Beaudoing, H. K., L'Ecuyer, T. S., Olson, W. S., Famiglietti, J. S., Houser, P. R., Adler, R., Bosilovich, M. G., Clayson, C. A., Chambers, D., Clark, E., Fetzer, E. J., Gao, X., Gu, G., Hilburn, K., Huffman, G. J., Lettenmaier, D. P., Liu, W. T., Robertson, F. R., Schlosser, C. A., Sheffield, J., Wood, E. F.: The Observed State of the Water Cycle in the Early Twenty-First Century. Journal of Climate, 28, 8289-8318, 2012.
Rohwer J, Gerten D, Lucht W. Development of functional irrigation types for improved global crop modelling. PIK Report 104, 2007.
Rost, S., Gerten, D., and Heyder, U.: Human alterations of the terrestrial water cycle through land management, Advances in Geosciences, 18, 43–50, 2008.
Samaniego, L. Kumar, R., Thober, S., Rakovec, O., Zink, M., Wanders, N., Eisner, S., Müller Schmied, H., Sutanudjaja, E.H., Warrach-Sagi K., and Attinger, S.: Toward seamless hydrologic predictions across spatial scales, Hydrology and Earth System Science, 21, 4323-4346, 2017.
Savenije, H. H. G.: The importance of interception and why we should delete the term evaporation from our vocabulary, Hydrological Processes, 18, 1507–1511, 2004.
Schewe, J., Heinke, J., Gerten, D., Haddeland, I., Arnell, N. W., Clark, D. B., Dankers, R., Eisner, S., Fekete, B. M., Colón-González, F. J., Gosling, S. N., Kim, H., Liu, X., Masaki, Y., Portmann, F. T., Satoh, Y., Stacke, T., Tang, Q., Wada, Y., Wisser, D., Albrecht, T., Frieler, K., Piontek, F., Warszawski, L., and Kabat, P.: Multimodel assessment of water scarcity under climate change, Proceedings of the National Academy of Sciences, 111, 3245–3250, 2014.
Sheffield, J., Wood, E. F., and Munoz-Arriola, F.: Long-Term Regional Estimates of Evaporation for Mexico Based on Downscaled ISCCP Data, Journal of Hydrometeoroly, 11, 253–275, 2010.

Siebert, S., Döll, P., Hoogeveen, J., Faures, J.-M., Frenken, K., and Feick, S.: Development and validation of the global map of irrigation areas, Hydrology and Earth System Science, 9, 535–547, 2005.
Siebert, S. and Döll, P.: Quantifying blue and green virtual water contents in global crop production as well as potential production losses without irrigation, Journal of Hydrology, 384, 198–217, 2010.
Siebert, S., Burke, J., Faures, J. M., Frenken, K., Hoogeveen, J., Döll, P., and Portmann, F. T.: Groundwater use for irrigation–a global inventory. Hydrology and Earth System Sciences, 14(10), 1863-1880, 2010.
Siebert, S., Henrich, V., Frenken, K., Burke, J.: Update of the Global Map of Irrigation Areas to version 5. Project report, 178 p., 2013.
Sloan, P.G. and I.D. Moore: Modeling subsurface stormflow on steeply sloping forested watersheds, Water Resources Research 20, 1815–1822, 1984.
Sperna Weiland, F. C., van Beek, L. P. H., Kwadijk, J. C. J., and Bierkens, M. F. P.: Global patterns of change in discharge regimes for 2100, Hydrology and Earth System Science, 16, 1047–1062, 2012.
Sterling, S. M., Ducharne, A., and Polcher, J.: The impact of global land-cover change on the terrestrial water cycle, Nature Climate Change, 3, 385–390, 2013.
Sutanudjaja, E. H., van Beek, L. P. H., de Jong, S. M., van Geer, F. C., and Bierkens, M. F. P.: Large-scale groundwater modeling using global datasets: a test case for the Rhine-Meuse basin, Hydrology and Earth System Science, 15, 2913–2935, 2011.
Sutanudjaja, E. H.: The use of soil moisture remote sensing products for large-scale groundwater modeling and assessment, PhD thesis, Utrecht Univ., Netherlands, 2012.
Sutanudjaja, E. H., van Beek, L. P. H., de Jong, S. M., van Geer, F. C., and Bierkens, M. F. P.: Calibrating a large-extent high-resolution coupled groundwater-land surface model using soil moisture and discharge data, Water Resources Research, 50, 687–705, 2014.
Sutanudjaja, E.H., van Beek, Rens, Wanders, Niko, Wada, Yoshihide, Bosmans, Joyce, Drost, Niels, van der Ent, Ruud, de Graaf, Inge, Hoch, Jannis, de Jong, Kor, Karssenberg, Derek, López López, Patricia, Peßenteiner, Stefanie, Schmitz, Oliver, Straatsma, Menno, Vannametee, Ekkamol, Wisser, Dominik and Bierkens, Marc: PCR-GLOBWB_model: PCR-GLOBWB version v2.1.0_beta_1, , doi:10.5281/zenodo.247139, 2017a.
Sutanudjaja, E.H., van Beek, Rens, Wanders, Niko, Wada, Yoshihide, Bosmans, Joyce, Drost, Niels, van der Ent, Ruud, de Graaf, Inge, Hoch, Jannis, de Jong, Kor, Karssenberg, Derek, López López, Patricia, Peßenteiner, Stefanie, Schmitz, Oliver, Straatsma, Menno, Vannametee, Ekkamol, Wisser, Dominik and Bierkens, Marc: PCR-GLOBWB 2 input files version 2017_11_beta_1, doi:10.5281/zenodo.1045339, 2017b.
The Global Runoff Data Centre (GRDC): The Global Runoff Database and River Discharge Data. 56068 Koblenz, Germany. Data were requested from http://www.bafg.de/GRDC and made available for us on 17 April 2014, 2014.
Todini, E.: The ARNO rainfall-runoff model, Journal of Hydrology, 175, 339–382, 1996.
Uppala, S.M. et al.: The ERA-40 re-analysis, Quarterly Journal of the Royal Meteorological Society 131, 2961–3012, 2005.
USGS EROS Data Center: HYDRO1k Elevation Derivative Database, LP DAAC: http://edcdaac.usgs.gov/gtopo30/hydro/, 2006.
Van Beek, L. P. H.: Forcing PCR-GLOBWB with CRU data, Tech. rep., Department of Physical Geography, Utrecht University, Utrecht, The Netherlands, http://vanbeek.geo.uu.nl/suppinfo/vanbeek2008.pdf, 2008.
Van Beek, L. P. H. and Bierkens, M. F. P.: The Global Hydrological Model PCR-GLOBWB: Conceptualization, Parameterization and Verification, Tech. rep., Department of Physical Geography, Utrecht University, Utrecht, The Netherlands, http://vanbeek.geo.uu.nl/suppinfo/vanbeekbierkens2009.pdf, 2009.
Van Beek, L. P. H., Wada, Y., and Bierkens, M. F. P.: Global monthly water stress: 1. Water balance and water availability, Water Resources Research, 47, W07 517, 2011.
Van Beek, L. P. H., Eikelboom, T., van Vliet, M. T. H. and Bierkens, M. F. P.: A physically based model of global freshwater surface temperature, Water Resources Research, 48, W09530, doi:10.1029/2012WR011819, 2012.
Van Vliet, M. T. H., Yearsley, J. R. F. Ludwig, Vögele, S, Lettenmaier, D.P. and Kabat, P.: Vulnerability of US and European electricity supply to climate change, Nature Climate Change, 2, 676–681, 2012.
Verdin, K.L., and Greenlee, S.K.,: Development of continental scale digital elevation models and extraction of hydrographic features. In: Proceedings, Third International Conference/Workshop on

Integrating GIS and Environmental Modeling, Santa Fe, New Mexico, January 21-26, 1996. National Center for Geographic Information and Analysis, Santa Barbara, California, 1996.
Vörösmarty, C. J., Leveque, C., and Revenga, C.: Millennium Ecosystem Assessment Volume 1: Conditions and Trends, chap. 7: Freshwater ecosystems, Island Press, Washington DC, USA, 165–207, 2005.
Wada, Y., van Beek, L. P. H., van Kempen, C. M., Reckman, J. W. T. M., Vasak, S., and Bierkens, M. F. P.: Global depletion of groundwater resources, Geophys. Res. Lett., 37, L20 402, 1-5, 2010.
Wada, Y., van Beek, L. P. H., Viviroli, D., Dürr, H. H., Weingartner, R., and Bierkens, M. F. P.: Global monthly water stress: 2. Water demand and severity of water stress, Water Resources Research, 47, W07 518, 1-17, 2011a.
Wada, Y., van Beek, L. P. H. and Bierkens, M.F P.: Modelling global water stress of the recent past: On the relative importance of trends in water demand and climate variability, Hydrology and Earth System Science, 15, 3785–3808, 2011b.
Wada, Y., van Beek, L. P. H., and Bierkens, M. F. P.: Nonsustainable groundwater sustaining irrigation: A global assessment, Water Resources Research, 48,1-18, 2012a.
Wada, Y., van Beek, L. P. H., Sperna Weiland, F. C., Chao, B. F., Wu, Y.-H., and Bierkens, M. F. P.: Past and future contribution of global groundwater depletion to sea-level rise, Geophysical Research Letters, 39, L09402, 1-6, 2012b.
Wada, Y., van Beek, L.P.H., Wanders N., and Bierkens, M.F.P.: Human water consumption intensifies hydrological drought worldwide. Environmental Research Letters 8, 034036, 2013.
Wada, Y., Wisser, D., and Bierkens, M. F. P.: Global modeling of withdrawal, allocation and consumptive use of surface water and groundwater resources, Earth System Dynamics, 5, 15–40, 2014.
Wada, Y., and M. F. P. Bierkens: Sustainability of global water use: past reconstruction and future projections, Environmental. Research Letters, 9, 104003, 2014.
Wada, Y., de Graaf, I.E.M., and van Beek, L.P.H.: High-resolution modeling of human and climate impacts on global water resources, Journal of Advances in Modeling Earth Systems, 8, 735–763, 2016.
Wanders, N., Wada, Y., and Van Lanen, H. A. J.: Global hydrological droughts in the 21st century under a changing hydrological regime. Earth System Dynamics, 6, 1–15, 2015
Wanders, N. and Wada, Y.: Decadal predictability of river discharge with climate oscillations over the 20th and early 21st century, Geophysical Research Letters, 42, 10689-10695, 2015
Wanders, N. and Wada, Y.: Human and climate impacts on the 21st century hydrological drought. Journal of Hydrology, 526, 208-220, 2016
Ward, P. J., Jongman, B., Sperna-Weiland, F., Bouwman, A., van Beek, L. P. H., Bierkens, M. F. P., Ligtvoet, W., and Winsemius, H.C.: Assessing flood risk at the global scale: Model setup, results, and sensitivity, Environmental Research Letters, 8, 044019, 2013.
Watkins, M. M., Wiese, D. N., Yuan, D.-N., Boening, C. and Landerer, F.W.: Improved methods for observing Earth's time variable mass distribution with GRACE using spherical cap mascons, Journal of Geophysical Research - Solid Earth, 120, 2648–2671, 2015.
Wesseling, C. G., Karssenberg, D., van Deursen, W. P. A., and Burrough, P. A.: Integrating dynamic environmental models in GIS: The development of a Dynamic Modelling language, Transaction in GIS, 1, 40–48, 1996.
Wiese. D.N.: GRACE monthly global water mass grids NETCDF RELEASE 5.0. Ver. 5.0. PO.DAAC, CA, USA. Dataset accessed [2017-09-15] at http://dx.doi.org/10.5067/TEMSC-OCL05, 2015.
Wiese, D. N., Landerer, F. W., and Watkins M. M.: Quantifying and reducing leakage errors in the JPL RL05M GRACE mascon solution, Water Resources Research, 52, 7490–7502, 2016.
Winsemius, H. C., Van Beek, L. P. H., Jongman, B., Ward, P. J., and Bouwman, A.: A framework for global river flood risk assessments, Hydrology and Earth System Science, 17, 1871–1892, 2013.
Winsemius, H. C., Aerts, J. C., van Beek, L. P., Bierkens, M. F.P., Bouwman, A., Jongman, B., Kwadijk, J. C., Ligtvoet, W., Lucas, P. L., van Vuuren, D. P., and Ward, P.J.: Global drivers of future river flood risk, Nature Climate Change, 6, 381–385, 2016.
Wisser, D., Fekete, B. M., Vörösmarty, C. J., and Schumann, A. H.: Reconstructing 20th century global hydrography: a contribution to the Global Terrestrial Network- Hydrology (GTN-H), Hydrology and Earth System Sciences, 14, 1–24, 2010.
Wood, E. F., Roundy, J. K., Troy, T. J., van Beek, L. P. H., Bierkens, M. F. P., Blyth, E., de Roo, A., Döll, P., Ek, M., Famiglietti, J., Gochis, D., van de Giesen, N., Houser, P., Jaffé, P. R., Kollet, S., Lehner, B., Lettenmaier, D. P., Peters-Lidard, C., Sivapalan, M., Sheffield, J., Wade, A., and Whitehead, P.: Hyperresolution global land surface modeling: Meeting a grand challenge for monitoring Earth's terrestrial water, Water Resources Research, 47, W05 301, 1-10, 2011.

List of Figures

Figure 8. a. Correlation between monthly TWS time series simulated PCR-GLOBWB 2 and the GRACE JPL PL-RL05M Mascon product over the period 2003-2015. b. Comparison of annual TWS series (inter-annual variability). Comparison is only done for the larger basins over 900,000 km2, conform the 3x3 arc-degree resolution of GRACE.

Fig. 9: Country water withdrawal (km^3/year) by source, evaluation of simulations with PCR-GLOBWB 2 with reported values in AQUASTAT (FAO, 2016). The scatterplots on the left (a, c, e) are for the period 1968-1992, while the right ones (b, d, f) are 1993-2015. The uppermost plots (a, b) are for total water withdrawal, the middle ones (c, d) are groundwater withdrawal, and the lowermost charts (e, f) are surface water withdrawal. Regression coefficient based on regression to non-log transformed data with intercept kept zero.

Fig. 10: Country water withdrawal (km3/year) by sector, evaluation of simulations with PCR-GLOBWB 2 with reported values in AQUASTAT (FAO, 2016). The scatterplots on the left (a, c, e) are for the period 1968-1992, while the right ones (b, d, f) are 1993-2015. The uppermost plots (a, b) are for withdrawal for agricultural purpose, the middle ones (c, d) are industrial withdrawal, and the lowermost charts (e, f) are domestic. Regression coefficient based on regression to non-log transformed data with intercept kept zero.

List of Tables

Table 1 - Global water balance components and human water withdrawal (in km^3/year and mm/year) over the period 2000-2015 as obtained from the 30 arc-minute and the 5 arc-minute simulations. The numbers are shown to high significance to show the water balance closure. This does not mean that we pretend to know e.g. global discharge with a km^3 accuracy (actual accuracy of the large fluxes is more in the order of 10^3 km^3)

		30 arc-min		5 arc-min	
		km^3/year	mm/year	km^3/year	mm/year
Global water balance	Precipitation	107452	808	107495	811
	Desalinated water use	3	0.02	2	0.01
	Runoff	42393	319	43978	332
	Evaporation*	65754	494	63974	483
	Change in total water storage	-693	-5	-455	-3
Groundwater budget	Groundwater recharge	27756	209	25521	193
	Groundwater withdrawal	737	6	632	5
	Non-renewable groundwater withdrawal (groundwater depletion)	173	1	171	1
	Renewable groundwater withdrawal	564	4	460	3
Withdrawal by sector	Agricultural water withdrawal (irrigation + livestock)	2735	21	2309	17
	Domestic water withdrawal	380	3	314	2
	Industrial water withdrawal	798	6	707	5
Withdrawal by source	Total water withdrawal	3912	29	3330	25
	Surface water withdrawal	3172	24	2697	20
	Desalinated water use	3	0.02	2	0.01
	Groundwater withdrawal	737	6	632	5

* Includes consumptive water use for livestock, domestic and industrial sectors

Table 2 - Groundwater withdrawal and total water withdrawal as compared to other studies (in km^3/year)

	Source	Year	Value (km^3/year)
Groundwater withdrawal	Wada et al. (2010) (from the IGRAC database)	2000	734 (±87)
	Döll et al. (2012)	1998-2002	571
	Döll et al. (2014) (their Table 2).	2003-2009	690-888
	Döll et al. (2014) (their Table 6).	2000-2009	665
	Pokhrel et al. (2015)	1998-2002	570 (±61)
	Hanasaki et al. (2018)	2000	789 (±30)
	This study (5 arc-minutes)	2000-2015	632
Total water withdrawal	Vörösmarty et al. (2005)	1995-2000	3560
	Oki and Kanae (2006)	contemporary	3800
	Döll et al. (2012)	1998-2002	4340
	Döll et al. (2014) (their Table 2)	2003-2009	3000-3700
	FAO (2016)	2010	3583
	Hanasaki et al. (2018)	2000	3628 (±75)
	This study (5 arc-minutes)	2000-2015	3330

Table A1 - List (non-exhaustive) of state and flux variables defined in PCR-GLOBWB

Description	Symbol	Unit
Interception storage	S_{int}	m
Snow cover/storage in water equivalent thickness (excluding liquid part S_{slq})	S_{swe}	m
Liquid/melt water storage in the snow pack	S_{slq}	m
Upper and lower soil storages	S_1 and S_2	m
Surface water storage (lakes, reservoirs, rivers and inundated water)	S_{wat}	m
groundwater storage (renewable part)	S_3	m
fossil groundwater storage (non-renewable)	S_{nrw}	m
total groundwater storage = $S_3 + S_{nrw}$	S_{gwt}	m
total water storage thickness = $S_{int} + S_{swe} + S_{slq} + S_1 + S_2 + S_{gwt}$	TWS	m
potential evaporation	E_{pot}	$m.day^{-1}$
evaporation flux from the intercepted precipitation	E_{int}	$m.day^{-1}$
evaporation from melt water stored in the snow pack	E_{slq}	$m.day^{-1}$
bare soil evaporation	E_{soil}	$m.day^{-1}$
transpiration from the upper and lower soil stores	T_1 and T_2	$m.day^{-1}$
total land evaporation = $E_{int} + E_{slq} + E_{soil} + T_1 + T_2$	E_{land}	$m.day^{-1}$
surface water evaporation	E_{wat}	$m.day^{-1}$
total evaporation = $E_{land} + E_{wat}$	E_{tot}	$m.day^{-1}$
direct runoff	Q_{dr}	$m.day^{-1}$
interflow, shallow sub-surface flow	Q_{sf}	$m.day^{-1}$
baseflow, groundwater discharge	Q_{bf}	$m.day^{-1}$
specific runoff from land	Q_{loc}	$m.day^{-1}$
local change in surface water storage	Q_{wat}	$m.day^{-1}$
total specific runoff	Q_{tot}	$m.day^{-1}$
routed channel (surface water) discharge	Q_{chn}	$m^3.sec^{-1}$
net fluxes from the upper to lower soil stores	Q_{12}	$m.day^{-1}$
net groundwater recharge, fluxes from the lower soil to groundwater stores	RCH = Q_{23}	$m.day^{-1}$
surface water infiltration to groundwater	Inf	$m.day^{-1}$
desalinated water withdrawal	W_{sal}	$m.day^{-1}$
surface water withdrawal	W_{wat}	$m.day^{-1}$
renewable groundwater withdrawal	W_3	$m.day^{-1}$
non-renewable groundater withdrawal (groundwater depletion)	W_{nrw}	$m.day^{-1}$
total groundwater withdrawal = $W_3 + W_{nrw}$	W_{gwt}	$m.day^{-1}$

Table A1 - continued

Description	Symbol	Unit
water withdrawal allocated for irrigation purpose	A_{irr}	$m.day^{-1}$
water withdrawal allocated for livestock demand/sector	A_{liv}	$m.day^{-1}$
water withdrawal allocated for agricultural sector = $A_{irr} + A_{liv}$	A_{agr}	$m.day^{-1}$
domestic water withdrawal	A_{dom}	$m.day^{-1}$
industrial water withdrawal	A_{ind}	$m.day^{-1}$

1336 *Table A2 - List of model inputs and parameters*

Description	Symbol	Unit	References/sources
Upper and lower soil store parameters:			FAO (2007) soil map; van Beek and Bierkens (2009)
- Soil thickness	Z_1 and Z_2	m	
- Residual soil moisture content	θ_{r-1} and θ_{r-2}	$m^3.m^{-3}$	
- Soil moisture at saturation	θ_{s-1} and θ_{s-2}	$m^3.m^{-3}$	
- Soil water storage capacity per soil layer: $SC = Z / (\theta_s - \theta_r)$	SC_1 and SC_2	m	
- Soil matric suctions at saturation	ψ_{s-1} and ψ_{s-2}	m	
- Exponent in the soil water retention curve	β_1 and β_2	dimensionless	
- Saturated hydraulic conductivities of upper and lower soil stores	K_1 and K_2	$m.day^{-1}$	
- Total soil water storage capacities = $SC_{upp} + SC_{low}$	W_{max}	m	
Land cover fraction: Land cover areas (including extent of irrigated areas) over cell areas	f_{lcov}	$m^2.m^{-2}$	GLCC v2.0 map (USGS, 1997); Olson (1994a, 1994b); MIRCA2000 dataset (Portmann et al., 2010), FAOSTAT (2012)
Topographical parameters:	DEM	m	HydroSHEDS (Lehner et al., 2008); Hydro1k (Verdin and Greenlee, 1996); GTOPO30 (Gesch et al., 1999)
- Cell-average DEM	DEM_{avg}	m	
- Flood plain elevation	DEM_{fpl}	m	

1337 *Table A2 - Continued*

Description	Symbol	Unit	References/sources
Root fractions per soil layer	Rf_{upp} & Rf_{low}	dimensionless	Canadell et al. (1996); van Beek and Bierkens (2009)
Arno scheme (Todini, 1999; Hagemann and Gates, 2003) exponents defining soil water capacity distribution	β_{arno}	dimensionless	Canadell et al. (1996), Hagemann et al. (1999); Hagemann (2002); van Beek (2008); van Beek and Bierkens (2009)
Ratio of cell-minimum soil storage to W_{max}	f_{wmin}	m	van Beek (2008); van Beek and Bierkens (2009)
Ratio of cell-maximum soil storage to W_{max}	f_{wmax}	m	van Beek (2008); van Beek and Bierkens (2009)
Parameters related to phenology			Hagemann et al. (1999); Hagemann (2002); van Beek (2008); van Beek and Bierkens (2009)
- Crop coefficient	K_c	dimensionless	
- Interception capacity	$S_{int-max}$	m	
- Vegetation cover fraction	C_v	$m^2.m^{-2}$	
Groundwater parameters			GLHYMPS map (Gleeson et al., 2014); van Beek (2008); van Beek and Bierkens (2009)
- Aquifer transmissivity	*KD*	$m^2.day^{-1}$	
- Aquifer specific yield	*Sy*	$m^3.m^{-3}$	
- Groundwater recession coefficient	*J*	day^{-1}	

Table A2 - Continued

Description	Symbol	Unit	References/sources
Meteorological forcing:			van Beek (2008); CRU (Harris et al., 2014); ERA40 (Uppala et al., 2005); ERA-Interim (Dee et al., 2011)
- Total precipitation	P	$m.day^{-1}$	
- Atmospheric air temperature	T_{air}	°C or K	
- Reference potential evaporation and transpiration	$E_{ref,pot}$	$m.day^{-1}$	
Others:			
- Non-irrigation sectoral water demand (i.e. livestock, dometic and industrial)		$m.day^{-1}$	Wada et al (2014)
- Desalinated water		$m.day^{-1}$	Wada et al., (2011a); FAO (2016)
- Lakes and reservoirs			GLWD1 (Lehner and Döll, 2004); GranD (Lehner et al., 2011)

1340